LAST LUMBAR FACET AND PEDICLE ORIENTATION IN ORTHOGRADE PRIMATES

By

DORION AMANDA KEIFER

A THESIS PRESENTED TO THE GRADUATE SCHOOL
OF THE UNIVERSITY OF FLORIDA IN PARTIAL FULFILLMENT
OF THE REQUIREMENTS FOR THE DEGREE OF
MASTER OF ARTS

UNIVERSITY OF FLORIDA

2005

For my mother and father and, of course, Mishka.

ACKNOWLEDGMENTS

I would like to thank, first and foremost, my committee, Drs. David Daegling and Michael Warren, for their support and guidance. The thoughtful insights of my committee made me think of this problem in new ways and were essential to the finished document. I would also like to thank Dr. Kenneth Mabry, Gary Sawyer, and Anita Caltabiano, from the Department of Anthropology, and Jean Spence, Teresa Pacheco, and Patricia Brunauer, from the Department of Mammalogy, at the American Museum of Natural History, for both the use of their collections as well as their encouraging words. A special thank you goes to Dr. Susan Anton at New York University for the use of her equipment; without her the data could not have been collected. I would like to thank Dr. Anthony Falsetti for the use of his equipment as well. The extra practice made all the difference. I thank the University of Florida Department of Anthropology staff, Karen Jones, Rhonda Riley, Patricia King, and LeeAnn Martin. I thank Shanna E. Williams for her artistic talent as well as her laughter. I would also like to thank Joseph, Jenna, and Maxine Coplin who moved me into their home for two months during data collection, as well as for their unwavering support. I thank Kristine Hulse, Jack Lackman, Linda Stanley and Mike Stanley, good neighbors and great friends. I would also like to thank Sandra Campbell, Sharon Milton-Simmons, Kelley Paulling, Jennifer Brookins, Mary Eckert, Renee Smith, Tina Sporer, and Barbara Young at the University of Florida of Florida, Department of Otolaryngology. They are the best coworkers anyone could ask for and they encouraged me every step of the way. I thank Dr. Jack Sedwick who has

been so supportive in this endeavor. Finally, I would like to thank my family: My mother and father, Pat and Orion Keifer, as well as my sisters Rachel McLaren, Megan Keifer, my brothers Orion (Paul) Keifer, Seth Keifer, and Chris McLaren, and last, but not least, my niece Maccayla Keifer.

TABLE OF CONTENTS

page

ACKNOWLEDGMENTS iv

LIST OF TABLES viii

LIST OF FIGURES ix

ABSTRACT x

CHAPTER

1. INTRODUCTION 1

The Two-Column Model of Force Transmission 3
Anthropological Research on the Primate Spine 7
Goals of the Current Project 12

2. PRINCIPLES OF FUNCTIONAL MORPHOLOGY 14

Phylogeny and Phylogenetic Constraint 14
Allometry 15
Ontogeny and Evolutionary Developmental Biology 15
Bone Biology and Behavior 16

3. RESEARCH DESIGN AND DATA COLLECTION PROCEDURES 19

Taxonomic Sample 19
Specimen Inclusion Criteria 21
Data Collection Instrumentation 22
Data Collection Procedures 23
Force Calculation: A Static Free Body Model 26
Statistical Testing 30

4. DATA TRANSFORMATION 33

Statistical Analysis and Results 46

Combining Mixed Sex Samples 46
Mean Directions and Mean Resultant Lengths 49
Pair-wise Testing 51

DISCUSSION 55

Pair-wise Testing 55
Pair-wise Comparisons and Phylogeny 56
Pair-wise Comparisons and Allometry 57
Pair-wise Comparisons and Bone Biology and Behavior 57
Force Transmission in the Posterior Elements 59
Feasibility of the Model 60
Vector Concentrations (MRL) 61
Facet Shape 61

CONCLUSIONS 63

MAJOR AXES-MINOR AXIS RATIO 66

ANGLE ERROR CALCULATION (DEGREES) 68

RAW VECTOR DATA TABLES 70

LIST OF REFERENCES 78

BIOGRAPHICAL SKETCH 84

LIST OF TABLES

Table page

1. Sample description. 21

2. Data transformation coordinate systems. 36

3. Pooling data, *Gorilla* sample. 48

4. Descriptive statistics. 49

5. Pair-wise results. 52

LIST OF FIGURES

Figure page

1. Potential forces acting on the right pedicle. 6

2. Facet shape. 25

3. Free body diagram.. 28

4. Normal vectors to the superior facets, right and left 29

5. Normal vectors to the inferior facets, right and left. 29

6. Axial vectors to the pedicles, right and left 29

7. Major axis vectors of the superior facets, right and left.. 31

8. Major axis vectors of the inferior facets, right and left 31

9. Major axis vectors of the pedicle, right and left 32

Abstract of Thesis Presented to the Graduate School
of the University of Florida in Partial Fulfillment of the
Requirements for the Degree of Master of Arts

LAST LUMBAR FACET AND PEDICLE ORIENTATION IN ORTHOGRADE PRIMATES

By

Dorion Amanda Keifer

May 2005

Chair: David J. Daegling
Major Department: Anthropology

The spine is critical for locomotor behavior. The spine is the foundational structure of the trunk and plays a key role in trunk position and stability. The spine also anchors major muscles of the forelimb and hindlimb, connecting them via a flexible column. Further, the spine articulates with the hindlimb, transmitting associated locomotor forces to the trunk. Despite the certain role of the spine in locomotion, the functional significance of vertebral variation is unestablished.

Morphological analyses of the primate spine indicate that the last lumbar vertebra posterior element morphology potentially correlates with locomotion. The calculation of the forces in the posterior elements of the last lumbar vertebra is necessary to demonstrate this connection. For the future development of a model for the calculation of these forces facet and pedicle orientation in the last lumbar vertebra were measured for four orthograde primates: *Homo sapiens, Gorilla gorilla, Pan troglodytes,* and *Pongo pygmaeus.*

Facet and pedicle orientation were described via six unit vectors for both the right and left side: normal to the superior and inferior facets, major axis of the superior and inferior facets, as well as axial to, and the major axis of, the pedicle. These vectors were calculated with respect to a vertebral reference axis, as well as the gravity vector when the spine is in orthograde posture. Descriptive statistics were calculated for all four species. Pair-wise tests were conducted among humans, gorillas, and chimpanzees.

The facet normal and pedicle axial vectors are essential for the development of a biomechanical model to estimate force direction in vertebral posterior elements. The statistical analysis of these vectors show they are very consistent within species, indicating that the mean vectors can be used for the future development of a biomechanical model. The pair-wise tests demonstrated that the species have statistically different mean directions.

The facet major axis vectors were calculated, as they may indicate the direction of the greatest range of motion in the facets. Generally, the descriptive statistics demonstrated that there was fairly large within species variability of these vectors. The pair-wise tests for equal mean direction indicated that, with a few exceptions, the species have statistically different mean directions with respect to these vectors.

The pedicle major axis vectors were calculated as they potentially indicate how the pedicle is oriented to resist bending force. The statistical data indicated that the orientation of these vectors is very consistent for the great apes tested. In contrast in humans, these vectors have greater variability though the functional significance of this is not clear. The intra-species pair-wise tests indicated that each species had a statistically different mean direction.

CHAPTER 1
INTRODUCTION

The study of the evolution of the relationship between form and function, or functional morphology, has long been of interest to anthropological researchers. Within functional morphology, the terms form and function are heuristic devices that allow the separation of phenomena that are inextricably linked within an organism. In general, form refers to shape and size, while function refers to how this form moves through space and how the form interacts with its surroundings. However, these two definitions do not have any real context unless they are applied to a specific problem involving an organism or group of organisms, (Wainwright, 1988). One such application explores the relationship between skeletal form and type of locomotion, including associated posture. Extant adult skeletal morphologies are not exclusively the product of body size but also of long histories of evolutionary changes, developmental processes, and daily activities. It is not easy to determine the extent of the individual contributions of these factors to the adult form, as they are interrelated parts of the total functional-morphological complex of an individual organism. Therefore, it is important to apply myriad techniques and perspectives to a specific problem.

The relationship between skeletal form and locomotion in extinct and extant primates has been a focus of study within the field of anthropology. Historically, these studies have centered on lower limb and pelvic morphology as well as the primate forelimb and shoulder girdle (Demes et al., 2000; Duncan et al., 1994; Heinrich et al., 1993; Hunt, 1991; Kimura, 2003; Latimer and Lovejoy, 1990a, 1990b; Lovejoy, 1975,

1979,1988; Ohman et al., 1997; Schmitt, 1994, 2003; Susman et al., 1984; Susman and Demes, 1994; Tuttle, 1985). However, these studies lacked an in-depth exploration of the spine as part of the functional complex of limb movement, ignoring the fact that "[a]mong mammals, structural differences of the lower precaudal spine correspond with contrasts between species in columnar function and positional behavior" (Sanders 1995: 97).

Recently, there have been a number of studies that address this gap in knowledge (Sanders, 1995, 1998; Shapiro, 1991, 1993, 1995; Shapiro and Johnson, 1998; Shapiro et al., 2001; Shapiro and Simons 2002; Velte 1987). These studies have revealed that the primate spine is morphologically conservative, despite quite dramatic differences in locomotor behavior. However, studies that compared the absolute and relative size and shape ratios of the posterior elements and pedicles of the primate spine have demonstrated morphological differences between bipedal and quadrupedal orthograde primates. This has lead to the speculation, though justifiably guarded, that these differences may represent differences in force transmission patterns in the posterior elements due to specific locomotor behavior. This conclusion is based upon traditional morphometric techniques that use size and shape ratios as proxy values for force magnitude and direction. This proves useful for locating possible areas where bone morphology may reflect function. An underlying assumption of previous primate spine morphometric studies is the assumption that the size of a given vertebral element is related to the magnitude of the forces acting upon that element (Davis, 1961: 337). However, this assumption may not always be reliable. Therefore, to examine this

relationship further, it is important to understand how force is transmitted and to calculate the magnitude of those forces using biomechanical principles.

The Two-Column Model of Force Transmission

Although there is a lack of biomechanically based studies that focus on non-human primate spines, the biomechanics of the human spine has been, and continues to be, the focus of a great number of studies. These studies were conducted for clinical (orthopaedics and orthopaedic surgery), occupational (ergonomics, proper lifting, etc.), military (human tolerance in operational and crash situations), and public safety purposes (seatbelt and other restraints, transportation safety, amusement rides). Given the large number of studies, it is impractical to exhaustively list all of them. Therefore, focus will be on research that is pertinent to the development of the two-column model of force transmission in the spine. The two-column model of force transmission is a general description of force transmission in the spinal column. The spine is comprised of two compressive columns called the anterior and posterior columns. The anterior column includes the vertebral bodies, intervertebral disks, and associated ligaments, while the posterior column is comprised the articular facets and the lamina and associated ligaments. The pedicles are the bony bridges that connect the two columns. These data will be presented prior to the discussion of past anthropological research, as it provides an analytical framework in which to evaluate the anthropological data, as well as defines crucial terminology.

The two-column pattern of force transmission is now widely accepted in the literature. However, prior to the 1960's, it was assumed that the pedicles and posterior elements did not transmit any significant force as they are smaller than the vertebral

bodies. They were believed to have three main purposes, to resist lateral rotation, to serve as muscle attachment sites, and to protect the spinal cord from trauma.

The first researcher to conclude that vertebral bodies could not be the sole means of force transmission was P.R. Davis in 1961. His conclusion was based upon a visual examination of human spinal morphology. Davis noted the area of the lumbar centra consistently increases in size from lumbar one to lumbar four. However, lumbar five, the last lumbar vertebra in humans, has a smaller lumbar centra than the vertebra above it. Davis concluded that if the vertebral bodies were the sole means of force transmission, the last lumbar centra would have to be larger than the one above it as the compressive force is cumulative. Based upon this observation, he concluded that the last lumbar vertebral body was subjected to less compressive force than the one above and posited that the compressive force was somehow resisted by the neural arch, which is comprised of the lamina and pedicles.

In 1974, Prasad and colleagues conducted a study to measure the role of the articular facets during acceleration. The researchers used several techniques to measure the load bearing capability of the facets in cadaveric studies. To qualitatively measure facet load, they attached strain gauges to the pedicles and lamina of their subject vertebrae. Quantitative measures of facet load were obtained using an intervertebral load cell that was designed to fit under the disk or vertebral body. The transducer was capable of measuring both axial force and the eccentricity of the axial force with respect to its geometric center. Cadavers were then accelerated in such as way as to simulate travel conditions experienced by U.S. Air Force pilots. Load cells were also mounted to the chair and restraint system. From this analysis, Prasad and colleagues proved both

qualitatively and quantitatively that the articular facets were involved in load transmission. However, they were unable to calculate the facet load.

In 1980, the work of Adams and Hutton filled in the information gap. They proved experimentally the significant role that articular facets play in forces transmission and also provided a measure of load transmission. Using "green" cadaver vertebral sections consisting of two vertebrae and the intervening disk, positioned as they would be *in vivo,* the researchers subjected the sections to compressive loads and various angles and measured deformation for acute loads and bone compression for constant loads. The load borne by the facets was shown to be posture dependent. They found facets withstand the highest force load when the body is in a standing, upright position. In this posture, facets transmit 16% of the total force load. This is the generally accepted number in the literature: however, some studies have placed this figure as high as 23% in the fifth (last) lumbar in humans (Pal and Routal, 1987).

In 1989, El-Bohy and colleagues' cadaveric studies demonstrated that the mechanism of posterior element load transmission was via facet/lamina contact by directly measuring contact pressure in the joints under various loading conditions using motion segments consisting of three vertebrae and their intervertebral disks. They measured contact pressure by placing a transducer between the inferior facets and the lamina of the vertebra below. Their results verified that loads passing through the facets are transmitted via contact between the facets and lamina.

Previous research confirms that the posterior elements are involved in force transmission. However, the magnitude, direction, and type of force acting on the individual posterior elements and pedicles are not known. There has been some

speculation as to the loading conditions of the pedicles. One hypothesis is that the pedicles are subjected to bending stresses as a result of muscles action on the spinous or transverse processes or alternately from the posterior elements (Bogduk and Twomey, 1987). It has also been suggested that the pedicles may be subjected to tension from the facets locking to prevent the vertebrae from sliding forward (Bogduk and Twomey, 1987). Finally, it has also been hypothesized that the pedicles may be subjected to compressive axial loads from the vertebral body to the lamina (Pal and Routal, 1986,1987). However, none of these hypotheses has been proven. There are four potential forces acting upon the pedicles: torsion, compression, bending and shear (Figure 1). In this figure compression is shown. Alternately, this force could be tension. The torsion is depicted as clockwise, however it may be counter clockwise. Similarly the bending and shear is depicted as an upward force. However, it may also be a downward motion.

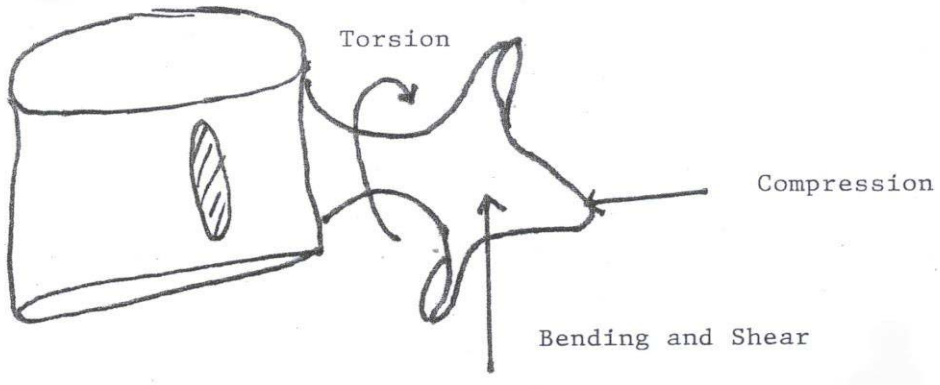

Figure 1. Potential forces acting on the right pedicle.

Anthropological Research on the Primate Spine

Three research studies were instrumental in the development of the current research design. Comparative studies on the primate spine indicated that biomechanical analysis of the posterior elements is important for understanding their role in posture and locomotion. The results of these three works and their relevance to the current problem are discussed in detail in the following section.

An early functional morphology study addressing the primate spine from a comparative perspective was Margaret Velte's (1987) dissertation that developed and described a biomechanical model for the anthropoid spine. Velte focused completely on the morphology of anterior vertebral elements, which are comprised of the vertebral centra, intervertebral disks, and associated ligaments. Her sample included *Alouatta, Ateles, Cebus, Cercopithecus, Homo, Gorilla, Pan*, and *Papio,* as well as some fossil material. The fossil material will not be discussed as it is beyond the scope of the current project. Further, the discussion will focus on results for the species included in the current study, *Homo, Gorilla,* and *Pan*.

Velte modeled individual vertebral bodies as short, deep beams. Using strength values of trabecular bone, she calculated the tensile and compressive bending moments and the shear force at failure. The shear and the bending moments were calculated for both dorsoventral flexion and lateral flexion axes. Her results indicate that shear and tensile stresses intensify along both axes. However, her data indicates that compressive stresses are reduced along the lateral flexion axis in cercopithecoids and along the dorsoventral flexion axis in hominoids. Velte concluded that the vertebral centra of *Homo*, *Gorilla*, and *Pan* are strongest in compression. Velte postulated that these data

indicate the hominoid pattern of short, broad vertebral centra is an adaptation to orthograde posture.

Liza Shapiro (1991,1993) also addressed the primate spine from a comparative perspective. Her extant sample also contained a large number of species including *Aloutta, Ateles, Cebus, Gorilla, Homo* (pygmy and non-pygmy), *Hylobates, Indri, Pan, Papio, Pongo, Propithecus,* and *Varecia*. Again, this discussion focuses on the species included in the present study, *Homo, Gorilla, Pan,* and *Pongo*.

Like Velte, Shapiro measured and evaluated vertebral centra. However, she also focused on the posterior elements and the pedicles. Shapiro's goal was to define aspects of vertebral morphology that were uniquely human. In order to accomplish this goal, she recorded various vertebral measurements: vertebral body (centra) area (calculated as an ellipse from the measured ventrodorsal and mediolateral distances at midpoint of the body), pedicle area (product of the length and width), pedicle shape (ratio of the width to the length), lamina area (product of the width and ventrodorsal thickness), and lamina shape (ratio of the lamina ventrodorsal thickness to the width). These metrics were selected to reflect the relative loads passing through the anterior and posterior columns. Finally, she measured the angulation of the superior facet (medial interfacetal width - lateral interfacetal width/2 times the facet width).

From the results of these measurements and calculations, Shapiro concluded, as compared to the great apes (*Gorilla, Pan*, and *Pongo*), humans have large vertebral centra (body) areas for their body weight. Shapiro speculated that this large body area may be related to increased compressive force associated with bipedalism. She did note that, like Velte, her studies indicated that humans and great apes have shorter, broader

vertebral bodies as compared to other primates. As mentioned, human vertebral body areas increase in size from the first to the penultimate lumbar vertebra; however, at the last lumbar level, the vertebral body area reduces in size. Once thought to be a uniquely human pattern, Shapiro's results indicate this pattern was found in nearly all the primates in her sample.

For both pedicle area and pedicle shape, her ANOVA tests indicated that *Homo, Gorilla, Pan*, and *Pongo* each have statistically different mean values. There were no statistically significant within species differences between male and female and therefore, for the all species, the sexes were pooled. Although each species had a unique mean for both pedicle area and pedicle shape, all four species trend toward increased pedicle area from the penultimate to last lumbar vertebrae. Shapiro speculated that this increased pedicle area is a function of the reduced vertebral body area of the last lumbar. Counter to speculation, this pattern is also seen in primates that do not have a reduced vertebral body area of the last lumbar vertebra. Shapiro also discerned that pedicle area is highly correlated with body size, with the notable exception of the last lumbar vertebra. At this level humans have a larger pedicle area than would be expected for their size. The results of pedicle shape (ratio of width to height) analysis indicate that, for humans, the increase in pedicle area at the last lumbar level occurs due to an increase in pedicle width relative to pedicle height. The *Pan, Pongo*, and *Gorilla* samples did not exhibit a pedicle shape change between the penultimate and last lumbar vertebrae. However, when compared with non-hominoids in her sample, the great apes and humans have short, wide pedicles.

On one hand, the human and great ape samples have similar trends in the lumbar region, with humans expressing these trends more dramatically. This would suggest that

this pattern is more likely related to postural behavior. On the other hand, the ANOVA test indicated the species have statistically different mean values, suggesting that each species has a unique posterior element morphology.

The ANOVA tests of lamina shape (ratio of ventrodorsal thickness and width) again indicate humans, gorilla, chimpanzees, and orangutan have unique mean values. As with the pedicle ANOVA test, males and females were pooled. Shapiro's results indicate that humans have wider lamina than the great apes. Further, human laminae become progressively wider, relative to thickness from lumbar one to the last lumbar. The gorilla, chimpanzee, and orangutan laminae to do not display this change.

Shapiro (1991) indicates that the laminae are an important aspect of posterior element force transmission because compressive force moves down the vertebral column via facet/lamina contact. The increasing width of lamina in humans may therefore be a reflection of increased compressive forces due to bipedal locomotion. Interestingly, despite great apes' orthograde posture, they do not share a similar pattern.

Finally, Shapiro (1991) measured facet angulation of the superior facets. The ANOVA test again indicated that the four groups have statistically different superior facet angulation means. As with the other ANOVA tests, males and females were not found to have any statistically significant differences and were pooled.

Despite statistically different mean values, general trends were found. For example, gorillas and chimpanzees demonstrated similar patterns, with superior facet angles becoming more acute from lumbar-one to the last lumbar, while humans facet angulations becomes more oblique. Orangutans appear to have a mean facet angle value at the last lumbar level that is identical to humans (i.e. laterally oriented), though facet

angles appear to follow the chimpanzee and gorilla pattern until the last lumbar level. Humans follow a pattern in which the superior facet angle becomes more oblique.

The angulations of the superior facets provide information about the lateral rotation permitted in the spine. The gorilla and chimpanzee facets seem oriented to restrict lateral rotation. The increasingly oblique angulations in humans have been posited to help resist forward displacement of the vertebrae as the last lumbar vertebra in humans is angled forward. Finally, the functional significance of the orangutan facet angulation pattern is not currently understood.

William Sanders (1995,1998) also conducted comparative morphological studies of the primate spine. The goal of his analysis was to use an extant primate sample to describe Australopithecine spinal biomechanics. He had a diverse sample, however I will only focus on the species relevant to the present study. Two of his measures are significant to the current problem, facet spacing and orientation and pedicular robustness and cross-section area.

With respect to facet angulation, Sanders'(1995;1998) data supported Shapiro's (1991;1991) finding. Like Shapiro, Sanders only documented facet angulation for the superior facets. However, Sanders (1995;1998) also highlighted facet spacing. Gorillas, chimpanzees, and orangutans have superior facet spacing that narrows slightly from the first to last lumbar vertebrae. In humans, the spacing between the superior facets increases from the first to last lumbar vertebrae. Sanders (1998) suggested that this pattern is important for spinal stability as more widely spaced facets create a more stable "base."

Sanders (1995;1998) also measured pedicle width and length to calculate pedicle area and robustness. Sanders' data indicate that ape pedicles are robust, shorter and wider, when compared to monkey pedicles. According to Sanders (1995;1998), muscle force accounts for part of the robustness as the transverse process of hominoids are rooted on the pedicles. However, Sanders (1995;1998) also documents scaling trends that indicate bending stresses as a critical factor for pedicular dimensions. From the first to last lumbar vertebra, great ape pedicles increase in width and decrease in length. Human vertebrae also follow this pattern; however, the last lumbar vertebra in humans has an extremely wide pedicle. These data are in agreement with Shapiro (1991;1993).

The results of the above research studies are not straightforward. On one hand, ANOVA tests indicate that for measures defined by the study each species had a statistically different mean value. However, the results also indicate that humans and great apes share generalized patterns of vertebral morphology. To further explore the functional morphology of the posterior elements it is necessary to develop a methodology to calculate the magnitude of stresses and strains on these elements. It is also desirable to measure and compare previously unmeasured variables. The current project addresses both of these issues.

Goals of the Current Project

The goal of this project is to document last lumbar facet and pedicle orientation in orthograde primates. These orientations were analyzed from two perspectives. First, descriptive statistics were calculated. Second, pair-wise tests for equal mean direction were conducted. The results indicate whether vectors means can be used to develop biomechanical models for force calculation in the last lumbar posterior elements. The results also indicate how orientation vectors vary among orthograde species with diverse

locomotor behavior. If current and future research on the posterior element morphology demonstrates that the morphology of the elements reflects postural and locomotor behavior, it will provide another method for elucidating postural and locomotor behavior in the fossil record.

CHAPTER 2
PRINCIPLES OF FUNCTIONAL MORPHOLOGY

Anthropological researchers rely heavily on skeletal material to make many inferences, such as taxonomy, evolutionary relationships, life history, and behavior. The current project's focus is the extent to which locomotor and positional behavior can be inferred from the posterior element morphology of the last lumbar vertebrae. The theoretical paradigm of functional morphology relies heavily on physics and engineering principles. Unlike engineered objects, however, the biological form is a product of many interrelated factors and processes: evolutionary history, growth and size, locomotor and postural behaviors, and so forth. There are four major areas in which the simple "form follows function" axiom of functional morphology is called into question. These major areas are phylogeny and phylogenetic constraint, allometry, ontogeny and evolutionary biology, and bone biology and behavior. However, the reader is cautioned that these categories, though artificially separated, are interrelated.

Phylogeny and Phylogenetic Constraint

The current form of any biological organism is constrained by their evolutionary, genetic history. The significance of this in terms of the current, and all, functional morphological studies is that aspects of the current morphology may not have functional significance. Rather they are simply a reflection of common ancestry and subsequent phylogenetic constraint. In order to elucidate which aspects of a species' morphology are likely related to phylogenetic constraint, a comparative sample is necessary. In this

study, a comparative sample of four closely related orthograde species with diverse locomotor repertoires was included.

Allometry

Allometry refers to changes in morphology that are not necessarily related to change in function but rather are "by products" of body size. In the present study, the methodology does not remove the factor of size in a meaningful way. Size is removed in the sense that the data are presented as unit vectors. Unit vectors do not, by definition, give any information regarding size as the vectors are divided by their length, resulting in all vectors having a length of one. Consequently, unit vectors only describe direction. Correcting for size is not appropriate in this case, as the goal is to determine orientation. The sample does include an extremely sexually dimorphic species, *Gorilla gorilla* as well as two similarly sized species, *Homo sapiens* and *Pan troglodytes*. Pair wise comparisons for equal mean direction were conducted between the male and female *Gorilla* vectors, as well as between *Homo* and *Pan.* The results of these tests will give some information regarding the dependence of the measured unit vectors on body size.

Ontogeny and Evolutionary Developmental Biology

Developmental processes affect the adult form in ways that may not be a reflection of function but rather are the results of canalization and developmental stability. The concepts of "[c]analization and developmental stability refer to the tendency of developmental processes to follow a particular trajectory despite external and internal perturbation," (Hallgrimsson et al., 2002: 131). Currently, there is no information in the literature that documents the extent to which posterior element vertebral morphology is constrained by canalization and developmental stability. This information is necessary to understand the functional morphology of the vertebral column, and it is expected that this

research will be conducted in the future. However, the reader is cautioned that the results of the current study were interpreted without the benefit of this information.

Bone Biology and Behavior

Studies of bone biology and bone behavior consider bone's response to the internal and external environment. The theory that "the distribution of strain trajectories engendered through functional activity is responsible for the development and maintenance of trabecular alignment and cancellous bone density within a bone" is the commonly accepted modern conceptualization of Wolff's law (Biewener et al., 1996: 1). This theory is very attractive in terms of functional morphological analyses because if it is correct, bone morphology can unproblematically be interpreted as a reflection of function. However, it is important to note, as Cullinane and Einhorn (2002) pointed out there are compelling critiques of theory (Bertram and Schwartz, 1991; Bienwener et al., 1996; Fyrie and Carter, 1986, Pearson and Lieberman, 2004) as well as scholarly debates about the mechanisms of the bones response to the mechanical environment (Martin, 2000; Mullender and Huiskes, 1995; Turner and Pavalko, 1998).

Generally, interpretations support that, in the course of normal loading during daily activities, the skeleton accumulates microscopic damage. The field of bone biology currently supports the theory that this microdamage triggers a remodeling response within the skeleton (Yerby and Carter, 2000). It is at this point, however, that dissension arises within the literature; bone tissue is not consistent or uniform in its response to stresses and strains. For example, a study that used a canine model resected the subjects' radii and allowed locomotion with the ulna supporting all the weight. The results of this study demonstrated a lack of uniform skeletal response as some of the subjects suffered fatigue fractures of the ulna, while others developed massive hypertrophy of the ulna

(Chamay and Tschantz, 1972). However, the results of this study are difficult to interpret. In the canine model the radius is much larger than the ulna. Therefore, the ulna was subjected to loading that would never be encountered outside of the research setting.

In a follow-up study, Carter and associates (1981) also used a canine model, but the ulna rather than the radius was resected. In this study, they found that bone formation in the radii was negligible. This would seem to indicate that the radius of the canine is overbuilt with respect to the forces that it must withstand.

To add another piece to this already difficult puzzle, fractures can occur at the upper levels of normal activity. For example, pars defects, fractures of the *pars inarticularis*, are a very common condition in humans, especially in the last lumbar vertebra (Burkus, 1988; Kip et al., 1994; Sermon and Spengler, 1981). Contrary to Wolff's Law, however, this shear fracture is not caused by a large acute stress to the *par inarticularis.* Rather this fracture occurs due to repetitive loading and subsequent fatigue failure. This fracture is often found in athletes.

A clear understanding of the cellular process by which bone repairs itself as well as bone as a biological material is essential to understanding how bone responds to the mechanical environment. However, it is not currently understood. The adult skeleton is in a constant state of deterioration and reformation by the osteoclasts and osteoblasts in trabecular surfaces and in Haversian systems. In simplified terms, when a microcrack forms in bone, osteoclasts activate on the crack surface resorbing the damaged bone. This activates the osteoblasts, which stimulate new bone growth (Brukner et al., 1999; Mundy, 1999; Schaffler, 2000). Colloquially, this is known as the "drill and fill" process. The intuitive and pervading opinion, until recently, was that the formation of microcracks is a

mechanical process in which microscopic fissures in the bone are formed faster than they can be repaired by the body. However, recent research indicates that stress fractures are a response to a positive feedback mechanism. The mechanism of increased usage stimulates bone turnover, which results in focally increased bone remodeling. It is theorized that increased bone porosity and bone mass result, weakening the bone (Brukner et al., 1999; Schaffler, 2000). In other words contra, to the current understanding of Wolff's Law, this theory indicates that when skeletal material is subjected to repetitive stresses and strains, it is ultimately weakened, not strengthened by the remodeling process.

Fortunately, more and more anthropological researchers are interested in moving beyond the Wolff's Law paradigm. Currently, the two most influential perspectives that move beyond this paradigm are bone developmental genetics and biomechanics (Pearson and Lieberman, 2004). The goal of this project is to move beyond morphological studies on the primate spine heavily reliant on Wolff's Law and develop biomechanically based research to further our understanding of spinal functional morphology.

CHAPTER 3
RESEARCH DESIGN AND DATA COLLECTION PROCEDURES

Taxonomic Sample

This research further explores the extent to which postural and locomotor behavior affects the morphology of the last lumbar posterior elements. The last lumbar vertebra was chosen as previous research has correlated statistical differences between species, suggesting that its morphology is most likely to reflect locomotor patterns (Shapiro, 1993). In order to determine if stresses and strains resulting from postural and locomotor behavior affect the morphology of the posterior elements, it is necessary to compare species with similar postural behavior but different locomotor repertoires. Four orthograde species with diverse locomotor behaviors were chosen for the study: *Gorilla gorilla, Pan troglodytes, Pongo pygmaeus,* and *Homo sapiens.* Locomotor behavior cannot accurately be described using gross categories such as "knuckle-walker." Despite the fact that primates generally have a dominant form of locomotion, they engage in diverse locomotor behaviors that should not be ignored. Outlined below are the locomotor behaviors of the orthograde species included in this study.

In the adult gorilla, terrestrial knuckle walking accounts for 94% of the distance traveled by mountain gorillas. They rarely engage in climbing (vertical) and engage in bipedalism, leaping, brachiation, or bridging even less frequently (Shapiro, 1991; see also Tuttle and Watts, 1985). Lowland gorillas appear to be more arboreal than mountain gorillas (Shapiro, 1991; see also Dixon, 1981; Fleagle, 1988). However, they were

included in the gorilla sample because "they feed, rest, and sleep on the ground where they move by quadrupedalism," (Shapiro, 1991: 17).

Pan troglodytes most frequently engage in knuckle-walking quadrupedalism. This locomotor behavior accounts for 86% of their locomotor activity. However, this species also engages in, from most to least frequent, quadrumanous climbing and scrambling (11%), arm swinging and bipedalism (1%), and leaping (< 1%). Only 16% of this species' locomotion is arboreal (Shapiro, 1991; see also Doran, 1989).

Pongo pygmaeus is the most arboreal of all the species included in the study. Quadrumanous scrambling is the most important locomotor behavior for this species. However, they also engage in the following behaviors, listed from most to least frequent: brachiation, tree swaying, quadrupedal walking, and climbing, (Shapiro, 1991, see also Sugardjito, 1982; Sugardjito and van Hooff, 1986).

Homo sapiens are the most orthograde of all the species included in the sample. They are capable of a variety of locomotor behaviors, such as walking, running, climbing, swimming, and hanging. However, bipedal walking is their single most important form of locomotion.

Table 1 describes the taxonomic sample for the study. As can be seen from the table the gorilla sample is comprised of 17 adult specimens of known sex. The chimpanzee sample is comprised of 18 adults specimens. There were 6 male specimens and 12 of unknown sex. The orangutan sample is quite small and consists of 4 male specimens and 1 specimen of unknown sex. The human sample consists of 19 adult specimens, 17 males and 2 females. The specimens were from an older population ($\bar{x}$ = 57.47 years, sd = 11.57years).

Table 1. Sample description.

Taxonomic Designation	Sex	Total
***Gorilla* Sample**		
Gorilla gorilla gorilla	Male	7
Gorilla gorilla gorilla	Female	6
Gorilla gorilla beringei	Male	2
Gorilla sp indent	Male	1
Gorilla sp indent	Female	1
Total		**17**
***Pan troglodytes* Sample**		
Species Designation	Sex	Total
Pan troglodytes	Male	6
Pan troglodytes	Unknown	12
Total		**18**
***Pongo pygmaeus* Sample**		
Taxonomic Designation	Sex	Total
Pongo pygmaeus	Male	4
Pongo pygmaeus	Unknown	1
Total		**5**

***Homo* sapiens Sample**				
Taxonomic Designation	Sex	Race	Decade of Life	Total
Homo sapiens	Male	White	Fifth	4
Homo sapiens	Male	White	Sixth	4
Homo sapiens	Male	White	Seventh	3
Homo sapiens	Male	White	Eighth	3
Homo sapiens	Male	White	Ninth	1
Homo sapiens	Male	Black	Fifth	1
Homo sapiens	Male	Black	Sixth	1
Homo sapiens	Female	White	Fifth	1
Homo sapiens	Female	Black	Seventh	1
Total				**19**

Specimen Inclusion Criteria

Specimens were collected from the American Museum of Natural History, Departments of Mammalogy and Anthropology. With the exception of two *Gorilla* specimens, all of the non-human specimens were collected from the Department of Mammalogy. The human specimens were collected from the Department of Anthropology's Morphology Collection.

Only adult specimens were included in the study. Adulthood was defined by epiphyseal fusion and dental criteria. Further, for the non-human primates only wild caught specimens were included.

Before collecting data, each specimen was carefully checked for breakage and pathology. Given the limited number of specimens available, a vertebra was not discarded outright for data collection if pathology, breakage, or cut marks were present. If the pathology was very limited data was not collected from the predetermined points on areas where the pathology was present. Similarly, if the vertebrae had breakage or were cut, data was not collected from the area with the breakage or cut marks. The *Pongo pygmaeus* sample posed a special challenge. It was noted by Schultz (1941) that even though *Pongo pygmaeus* can be said to reach adulthood by dental criteria it is possible that the epiphyses can remain unfused. In the present study, dental criteria were used to define orangutan adults, however specimens were rejected if the last lumbar vertebra showed incomplete epiphyseal fusion. This criterion severely limited the *Pongo pygmaeus* sample size.

Data Collection Instrumentation

Digitized three-dimensional coordinates of predetermined points were taken on a Microscribe® model 3DX (Immersion Corporation, 801 Fox Lane, San Jose, California 95131). At the beginning of each data collection session, Accuracy Check #1 and Accuracy Check #2, two calibration procedures recommended by the manufacturer were performed.

Accuracy Check #1 describes the Microscribe® position prior to turning it on. The Microscribe® performs a "self calibration" based upon the position at start up. Prior

to each measurement session, the Microscribe® was positioned carefully to correspond with the "home" position prior to turning it on.

Accuracy Check #2 required the program MSTest. This test procedure ensures that the joint encoders are working properly. MSTest gives joint angles for various stylus positions, which must be matched up to charts detailing the expected angles.

Finally, the Microscribe® 3DX has a "moveable" coordinate system. The X and Y axis are determined by the position of the swiveling arm at start up. Therefore, the Microscribe® was positioned consistently throughout the measurement procedure.

The data points were imported directly into a Microsoft Excel spreadsheet via Inscribe software. Linear measurements were made using a Mitutoyo digital caliper, model 573-225-10 (Mitutoyo American Corporation, 965 Corporate Boulevard, Aurora Illinois 60504). The digital caliper was zeroed and internally calibrated, in accordance with the operating manual, before each use.

Data Collection Procedures

The posterior element morphology of the vertebrae samples was documented via thirty-eight landmark points. The superior and inferior vertebral centra (body) surfaces were documented via five points each: the most anterior point at the midline, the most posterior point at the midline, the most lateral point in the mid-coronal plane on the right side, the most lateral point in the mid-coronal plane on the left, and the center point. Each facet had 5 landmark points for a total of 20 points. The center point was defined as an average of height and width. The four additional points were defined as the articular surface end points of the minor and major axes. Finally, the pedicles were defined by four points each: on the superior surface, at the midline, on the inferior surface, at the

midline, on the medial surface, in the midtransverse plane, and on the lateral surface, in the midtransverse plane.

For the purpose of replicability and consistency, each point was located and marked. The measurements required to locate the landmarks were documented using a Mitutoyo digital caliper (accurate to 0.01mm), when possible. Some points were recorded by sight, as accurate measurements were not possible with the calipers. This occurred when the element of interest was so small that accurate measurements could not be obtained. When this occurred, following the detailed measuring procedure would be sufficient to produce consistent measurements from observer to observer as the vertebral elements involved are extremely small. All measurements were taken at least two times and were accepted if the two values were within 0.05mm. The two accepted values were then averaged. The procedures used to locate the landmark points for each vertebral element are outlined below.

The vertebral body landmark points were located first. The center point was calculated using the measured values of vertebral width at the widest lateral point and anterior-posterior depth at the centerline of lateral symmetry. Once this point was located, a perpendicular set of axes was drawn on the vertebral body using a straight edge, aligned with the anterior-posterior centerline. The four additional points were located at the points were these axes intersected the edge of the vertebra superior vertebral body.

The facets points were located by first measuring the facet height and width. It should be noted that the author found that facet morphology varied greatly; however, the morphology could be divided into five general types as shown in Figure 1. The center

was located by taking half the value of both the measured height and width, and positioned in accordance with Figure 2. Once the center point was located, the center point as well as the facet shape category was used to define the major axis of the facet. Once the major axis was located, the minor axis was defined as the line perpendicular to the major axis, passing through the center point. The intersections of these axes with the edge of the facet defined the four additional points. The focus of this project is the major axis orientation. However the extent to which the major axis is larger than the minor axis may be of interest to the reader. Therefore, this value was calculated as the base ten logarithm of the ratio of the major to minor axis and is included in Appendix 1.

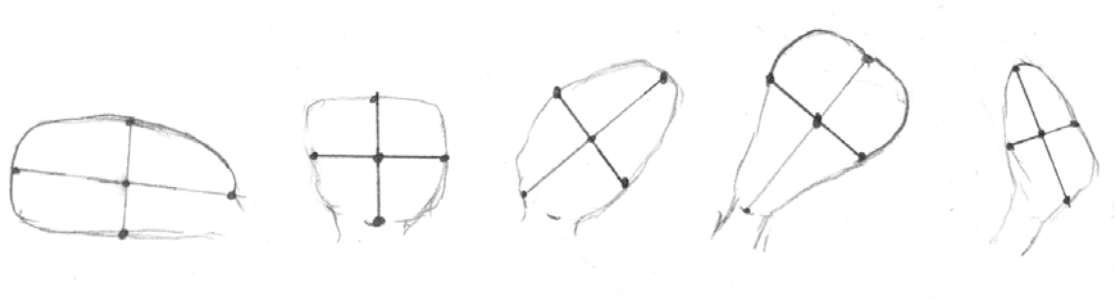

Figure 2. Facet shape. This figure shows the five major facet shapes that were seen during data collection, as well as the how the minor and major axes were drawn for each shape. From left to right, Type I, Lateral Oval, Type II, Square, Type III, Diagonal Oval, Type IV, Pear, and Type V, Kidney.

The pedicle landmark points were defined for the axial center of the pedicle, between the vertebral anterior body and the lamina. The specific points were defined as the middle point of each the superior, lateral, and inferior surface, again using height and width measurements. The medial point had to be located visually as the calipers did not fit into the neural canal. In order to improve the accuracy and consistency a method for locating the medial point was developed. The midpoint of the medial pedicle was located for both the superior and inferior surface. A line was then drawn to connect the two

points. This line was then used as a guide to locate the medial point. These points define the plane perpendicular to the axial line. Defining the exact center of the superior-inferior plane is not as critical as defining the lateral-medial center, which was accomplished using the above methodology.

Once all the landmark points were measured and marked, each vertebra was placed on a ring-stand, anterior side down, and superior side away from the ring-stand stanchion and secured by dental wax. The specimen cannot be moved during data collection as all landmarks were measured with respect to the origin of the Microscribe®. The relative position of the Microscribe® allowed access to all the landmark points on the vertebra to be measured without moving the vertebra. The axes of the Microscribe® was approximately aligned with the natural axes of the vertebra, such that the x, y and z axes of the Microscribe® approximated the superior-inferior, anterior-posterior and lateral axes of the vertebra, respectively. All vertebrae were measured with a similar orientation to the digitizer. On all specimens, the landmark points were recorded in the same order. Further, for each specimen the landmark points were measured at least two times in order to calculate an error rate.

Force Calculation: A Static Free Body Model

Analysis of the forces within the various elements within the vertebra is dependent on all external forces acting on the vertebra. From mechanics, these forces are depicted using a static free body diagram. The static free body diagram is an accepted and widely used methodology in biomechanics (see Panjabi and White, 2001 and Ozkaya and Nordin 1998, for fundamental biomechanics techniques). A two dimensional static free body diagram, as depicted in Figure 2, has been developed by the author to as a simplified starting point for the determination of the forces within the vertebral posterior elements.

As can be seen from the figure, the vertical force on the vertebra from the body above is supported by the forces from the inferior disk and the inferior facets. To determine how the force is transmitted, it is necessary to document the size and orientation of the load bearing surfaces and the elements of interest for calculations of the load. Sizes of various vertebral elements have been extensively documented as previously discussed. Orientation of the facets and pedicles can be documented via three-dimensional vectors, which is key for determining the angles in the static free body method. It is important to stress, however, that the static free body model is a simplified starting point that operates under certain assumptions. First, the model assumes that the force on the facets can be accurately modeled as normal to the center of the facet. The initial model does not contain any information regarding muscle force or ligaments. The work of Frank Holdsworth (1963) demonstrated that the posterior element ligaments are essential to stability in the spine. Finally, the accuracy of the model is dependent upon the accurate knowledge of the vertebra's *in vivo* position.

Fortunately, a study conducted by Albert Schultz and colleagues validated a biomechanical model for the calculation of load on the lumbar spine. In this study they compared values predicted by a biomechanical model to intradiscal pressure and myoelectric signals. They also correlated the effects of intraabdominal pressure on spinal loading. Their results indicate that a biomechanical model is "valid in the [loading] situations that were examined," (Schultz et al., 1982: 717). They also measured intraabodominal pressure and concluded, "the intraabdominal pressured were not large and seldom had a major influence on the overall mechanics of the trunk," (Schultz et al., 1982: 720). Given these conclusions, a biomechanical model that takes into account

vertebral geometry and muscle action should be an accurate predictor of the loads borne by the spine.

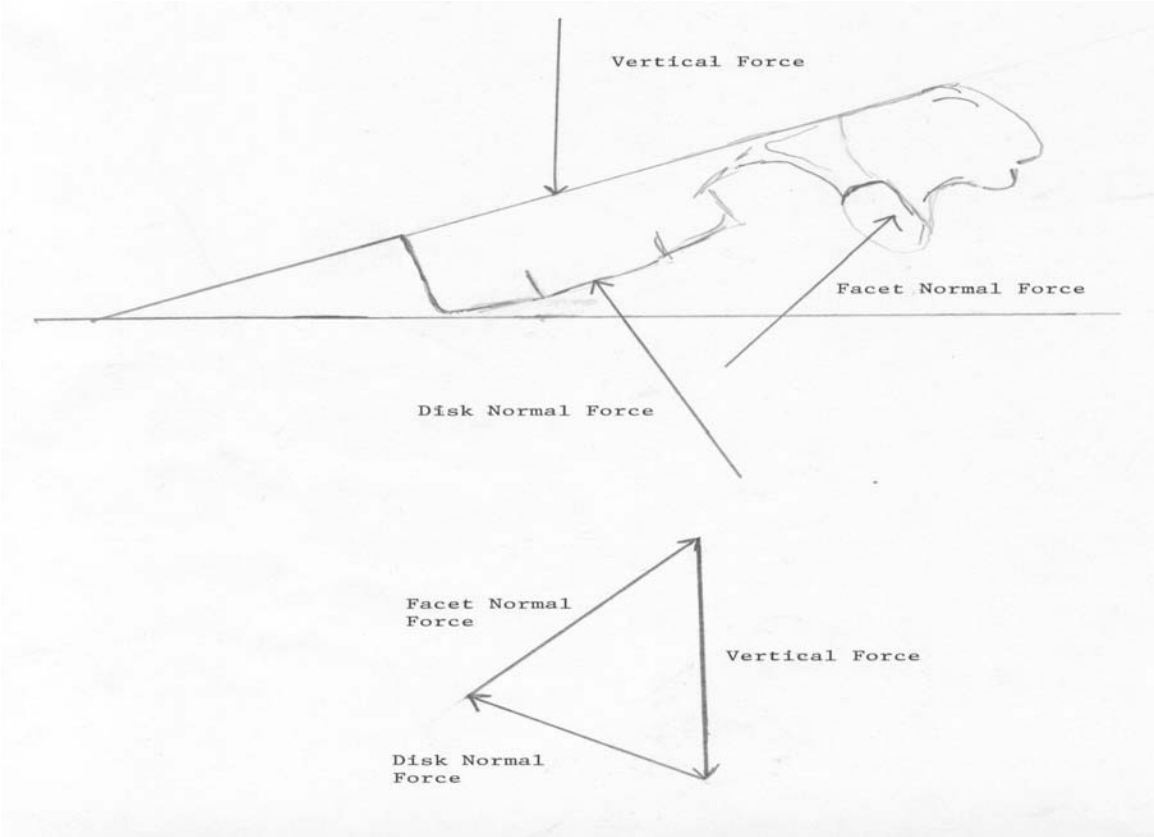

Figure 3. Free body diagram. This figure depicts a two-dimensional free body diagram. This is a simplified depiction of forces acting on the inferior facets. However, the figure clearly demonstrates the necessity of facet and pedicle orientation for force calculation. (Source: Drawn by Author).

The vectors needed to develop the free body model are described below:

1. The unit vector normal to superior facet. This is the vector normal to the center of the superior facet, divided by the vector length (Figure 4).

2. The unit vector normal to inferior facet. This is the vector normal to the center of the inferior facet, divided by its length (Figure 5).

3. The unit vector in the axial direction of pedicle. This vector describes the axial direction of the pedicle vector, divided by its length (Figure 6).

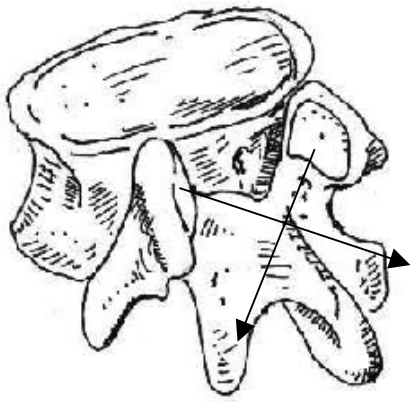

Figure 4. Normal vectors to the superior facets, right and left (Source: Shanna E. Williams.)

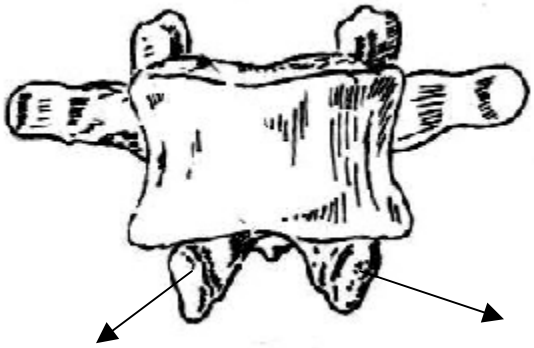

Figure 5. Normal vectors to the inferior facets, right and left (Source: Shanna E. Williams).

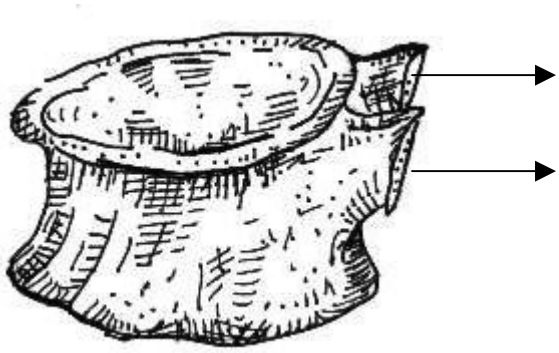

Figure 6. Axial vectors to the pedicles, right and left (Source: Shanna E. Williams)

The above vectors can be calculated for individual specimens. However, it is desirable to develop general species models. In order for such a generalized model to be possible, it is necessary that for each vector a species mean direction and mean resultant length is found. This is the measure of concentration, analogous to a standard deviation, which describes vector concentration as a value between zero and one. A value of one indicates a high concentration, i.e. all vectors are parallel and a value of zero indicates no concentration and randomly orientated vectors. The mean resultant length is an extremely important measure with respect to the development of species models. A low concentration would indicate that there is great within species variation with respect to vector direction. This in turn indicates that the mean value lacks any real meaning. A high concentration indicates that there is a true species mean, which can be used to develop species specific models.

Statistical Testing

The second goal of this project is to analyze the mean and variance of facet and pedicle orientation. The vectors that were calculated for the static free body diagram were also subjected to statistical analysis, as these vectors are crucial to the calculation of stresses and strains in the vertebrae. However, additional vectors were calculated, as they may be biomechanically significant. These vectors were the superior and inferior major axis vectors and the pedicle major axis vectors. The facets potentially allow sagittal, lateral, and axial rotation. The major axis of the facet may indicate the direction in which the facets allow the most rotation.

The pedicle is the bony bridge between two compressive columns and it has been hypothesized to be subject to bending moments. The major axis indicates the direction

on which the pedicle is oriented to resist the most bending force. However, it has not been conclusively proven that the pedicles are subject to bending forces.

4. Major axis of the superior facet. This is the vector with the larger magnitude between either the superior-inferior axis vector of the superior facet or the lateral-medial axis vector of the superior facet. The vector is then divided by its length in order to transform it into a unit vector. (Figure 7)

5. Major axis of inferior facet. This is the vector with the larger magnitude between either the superior-inferior axis vector of the inferior facet or the lateral-medial axis vector of the facet. The vector is then divided by its length in order to transform it into a unit vector. (Figure 8).

6. Major axis of pedicle at midpoint. This is the vector with the larger magnitude between either the superior-inferior axis vector at the midpoint of the pedicle or the lateral-medial axis vector at the midpoint of the pedicle. The vector is then divided by its length in order to transform it into a unit vector. (Figure 9).

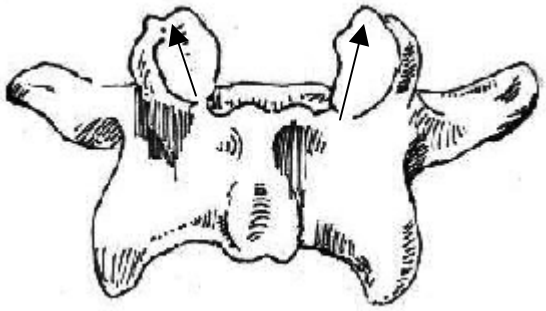

Figure 7. Major axis vectors of the superior facets, right and left. (Source: Shanna Williams).

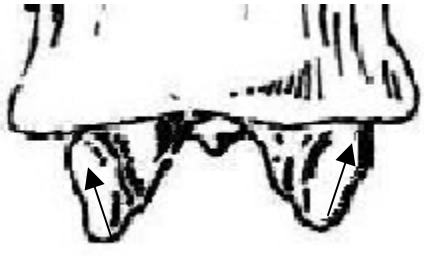

Figure 8. Major axis vectors of the inferior facets, right and left. (Source: Shanna E. Williams)

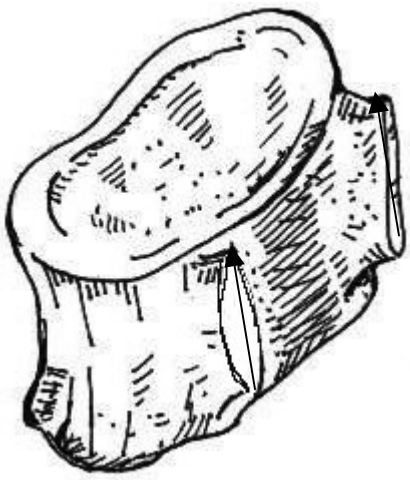

Figure 9. Major axis vectors of the pedicle, right and left. (Source: Shanna E. Williams)

The calculation and analysis of the above vectors will further our understanding of the relationship of posterior element morphology and posture and locomotion. Further, it is a first step in the development of a model to calculate actual stresses and strains in the posterior elements. This information will enrich our knowledge with respect to the relationship of posterior element morphology to load bearing.

CHAPTER 4
DATA TRANSFORMATION

In order to document the orientation of the facets and pedicles, it is necessary to record each vertebra's morphology, as expressed by the 38 landmark points, in three-dimensions. Fortunately**,** recent advances in computer technology have made this possible and have given anthropological researchers a new tool with which to study the skeletal form. The digitizer, in this case a Microscribe® 3DX, records x, y, and z coordinates with respect to its own origin. Using the information provided by the digitizer, the researcher must transform the data into useful information. In this study, the goal, of course, is to transform the coordinate data into unit vectors that describe facet and pedicle orientation with respect to a common coordinate system. This chapter describes in detail how a coordinate system for the vertebra was selected and how the measured quantities were transformed to the coordinate system.

The transformation process relies on three concepts from vector algebra; determining a vector from two points in space, the concept of a unit vector and, a vector multiplication operation (cross product).

Given point 1 in space with coordinates (x_1,y_1,z_1) and point 2 with coordinates (x_2,y_2,z_2) the vector $\vec{a}$, from point 1 to point 2 is found as follows:

$$\vec{a} = (x_2 - x_1)\vec{i} + (y_2 - y_1)\vec{j} + (z_2 - z_1)\vec{k}$$

Where $\vec{i}, \vec{j},$ and $\vec{k}$ are unit vectors in the x, y and z directions, respectively.

Substituting in a_x, a_y and a_z for $(x_2 - x_1)$, $(y_2 - y_1)$, and $(z_2 - z_1)$, the vector becomes:

$$\vec{a} = (a_x)\vec{i} + (a_y)\vec{j} + (a_z)\vec{k}$$

Because $\vec{i}, \vec{j},$ and $\vec{k}$ are all mutually orthogonal, Pythagorean Theorem can be used to determine the length of vector $\vec{a}$ between point 1 and point 2, as follows:

$$|\vec{a}| = \sqrt{(a_x)^2 + (a_y)^2 + (a_z)^2}$$

Vectors and their multiples all have the same direction. If one were to multiply a vector by the ratio of one to its length, the vector would have the same direction but would have a length of one. This is the definition of a unit vector. Mathematically, it can be expressed as follows:

$$\vec{a}_{unit} = \frac{\vec{a}}{|\vec{a}|} = \left(\frac{a_x}{|\vec{a}|}\right)\vec{i} + \left(\frac{a_y}{|\vec{a}|}\right)\vec{j} + \left(\frac{a_z}{|\vec{a}|}\right)\vec{k}$$

The third vector algebra concept, the cross product, can be expressed in two ways as follows:

$$\vec{a} \times \vec{b} = \vec{n}\,|\vec{a}|\,|\vec{b}|\sin\theta$$

Where: $\vec{a}$ = vector $\vec{a}$ with magnitude $|\vec{a}|$

$\vec{b}$ = vector $\vec{b}$ with magnitude $|\vec{b}|$

$\vec{n}$ = vector normal (perpendicular to both vectors $\vec{a}$ and $\vec{b}$ with magnitude 1)

θ = angle between vectors a and b.

The cross product can also be calculated using the determinant, as follows:

$$\vec{a}\ X\ \vec{b} = \begin{vmatrix} \vec{i} & \vec{j} & \vec{k} \\ a_x & a_y & a_z \\ b_x & b_y & b_z \end{vmatrix}$$

$$\vec{a}\ X\ \vec{b} = (a_y b_z - a_z b_y)\vec{i} + (a_z b_x - a_x b_z)\vec{j} + (a_x b_y - a_y b_x)\vec{k}$$

Where: $\vec{a}$ = vector $\vec{a}$ with magnitude $|\vec{a}|$

$\vec{b}$ = vector $\vec{b}$ with magnitude $|\vec{b}|$

$\vec{i}, \vec{j}$, and $\vec{k}$ = vectors with magnitude 1 in the x, y and z directions respectively

a_x, a_y, and a_z, = components of vector $\vec{a}$ in the x, y and z directions respectively

b_x, b_y, and b_z, = components of vector $\vec{b}$ in the x, y and z directions respectively

The first mathematical expression shows that the magnitude of the cross product is equal to the product of three variables, the magnitude of vector $\vec{a}$, the magnitude of vector $\vec{b}$, and the sine of the angle between vector $\vec{a}$ and vector $\vec{b}$. Of note, directional vectors are not necessarily tied to a particular point in space, that is all parallel vectors have the same directionality; however, an important consequence of the cross product calculation is that vector $\vec{a}$ and vector $\vec{b}$ are visualized as coplanar. The family of parallel planes containing the two vectors can be uniquely defined by the normal vector perpendicular to both vector $\vec{a}$ and vector $\vec{b}$.

The second expression of the cross product gives the vector in its coordinate form. As stated previously, our data is in the form of x, y, and z coordinates. The coordinates can also be thought of as a vector from the origin to the coordinate of the point. Therefore, vectors from the origin can be expressed as their x, y, and z coordinates which

are represented as a_x, a_y, and a_z for vector $\vec{a}$ and b_x, b_y, and b_z for vector $\vec{b}$. These values can be used in the cross product calculation.

The goal of the data transformation procedure was to determine three-dimensional coordinates of the measured points with respect to a defined coordinate system based on the morphology of the specimen. The initial step in this process was to choose the specimen-referenced axes. The axes that were chosen has the x direction in the anterior-posterior (anterior positive) direction, the y direction was in the right to left lateral (left positive) direction, and the z direction was in the superior-inferior (vertical) direction (up positive) of the main body of the vertebra.

Several translations and rotations of one coordinate system to the next were required, beginning with the coordinate system of the Microscribe® and ending with the gravity vector referenced coordinate system. Several intermediate coordinate systems were also required. The various coordinate systems are summarized in Table 2.

Table 2. Data transformation coordinate systems.

Coordinates	Nomenclature	Change from previous coordinate system
X,Y, & Z	Microscribe® referenced	Data as originally recorded
X,**Y**, & **Z**	Intermediate	Axes changed to approximate specimen referenced axes
$\mathbf{X_1}$,$\mathbf{Y_1}$, & $\mathbf{Z_1}$	Intermediate	Move origin to approximate sample referenced origin
$\mathbf{X_2}$,$\mathbf{Y_2}$, & $\mathbf{Z_2}$	Intermediate	Rotated about $\mathbf{Z_1}$ axis by the first Euler angle ϕ
$\mathbf{X_3}$,$\mathbf{Y_3}$, & $\mathbf{Z_3}$	Intermediate	Rotated about $\mathbf{X_2}$ axis by the second Euler angle θ
$\mathbf{X_4}$,$\mathbf{Y_4}$, & $\mathbf{Z_4}$	Intermediate	Rotated about $\mathbf{Z_3}$ axis by the third Euler angle ψ
x, y, & z	Sample referenced	Translate origin to center of inferior body
x_1, y_1, & z_1	Gravity referenced	Rotated about **y** axis by inferior body-horizontal angle ω

The Microscribe® records points with respect to its internal reference axes. Therefore, the specimen being digitized cannot be moved with respect to the digitizer reference during the digitizing process. In order to collect all the points of interest to the

study, it was necessary to have the anterior surface of the body in the approximate direction of the digitizer's Z axis, while the superior surface approximated the digitizer's Y axis and the lateral portions of the vertebra approximated the digitizer's X axis. The first step was to switch the axes nomenclature from that of the Microscribe® to that approximating the vertebral axes. The resulting renamed vector increases in the **Z** direction corresponding to increases in the superior direction and increases in the **X** direction corresponding to increases anteriorially. This was accomplished by changing the (X, Y, Z) nomenclature to the approximate vertebral reference axis (**X**, **Y**, and **Z**), as follows:

- **X**-axis values for the approximate vertebral coordinate system were set as the negative of the measured Z values
- **Y**-axis values for the vertebral coordinate system were set as the measured X values.
- **Z**-axis values for the vertebral coordinate system were set as the negative of the measured Y values.

The next step for aligning the specimens was to reference the data to an origin point on the vertebra. For this study, the center point of the inferior body was chosen. Though this designation is somewhat arbitrary, this point was chosen for ease of data interpretation. Problematically, however, the inferior surface of a vertebra is asymmetrical and is not a flat surface. It was necessary to correct for these limitations when locating the origin point in the three directions. For the y-direction, the origin was selected as a point halfway between the measured left and right landmark points. In the x direction the origin point selected was half way between the ventral and dorsal landmark points. The remaining point, in the z direction, was defined as the average of the four measured landmark points (left, right, ventral and dorsal). The appropriate center coordinate was subtracted from the data in the **X**,**Y**,**Z** coordinate system to determine the

coordinates in the new $\mathbf{X_1}$, $\mathbf{Y_1}$, $\mathbf{Z_1}$ intermediate coordinate system. This essentially translated the origin from that defined by the Microscribe® to a point that approximates the center of the inferior vertebral centra (body). The asymmetry of the vertebra may introduce a slight error with respect to the coordinate system. However, subsequent rotations will not produce additional error.

Once the data were translated to the approximate vertebral coordinate system and referenced to the approximate vertebral origin, it was then necessary to rotate the data. This step is very important because although every effort was made to consistently line up the individual specimens with the axis of the Microscribe®, rotational misalignment of a few degrees was unavoidable and is almost certainly inconsistent from sample to sample. To correct the misalignment, the data was rotated to correspond to the selected vertebral reference system using Euler angles. The "x convention" for Euler rotation is used.

The Euler angle rotation formula requires three distinct rotations. First, the coordinates are rotated about the **Z-axis,** then about the **X-axis,** and about the **Z-axis** a second time.

For the first rotation, the data were referenced to an intermediate axis ($\mathbf{X_2}$, $\mathbf{Y_2}$, and $\mathbf{Z_2}$). The data were rotated an angle ϕ about the $\mathbf{Z_1}$-axis such that the $\mathbf{X_2}$ axis is contained in both the $\mathbf{X_1}$-$\mathbf{Y_1}$ plane of the old coordinate axes and the x-y plane of the vertebra referenced axis. The data are then referenced to a second intermediate coordinate axes system ($\mathbf{X_3}$, $\mathbf{Y_3}$, and $\mathbf{Z_3}$). For this rotation, the vertebra is rotated an angle θ about the $\mathbf{X_2}$ axis such that the $\mathbf{X_3}$- $\mathbf{Y_3}$ plane of the intermediate coordinate axes system coincides with the x-y plane of the vertebra reference system, or stated another way, such that $\mathbf{Z_3}$

coincides with the z-axis of the vertebra reference system . Finally, the data are referenced to the vertebra reference system (x, y, and z) by rotating an angle ψ about the $\mathbf{Z_3}$ axis to bring the $\mathbf{Y_3}$ axis parallel with the y-axis in the vertebral reference axis.

In order to use the Euler Angle Rotation procedure, it is necessary to calculate the Euler angles (ϕ, θ, and ψ). Fortunately, the vectors necessary for this calculation can be derived directly from the data taken and the three vector algebra concepts noted above. Recall that one property of the cross product calculation is that it can be used to determine a vector that is perpendicular to both vectors used in the cross product. Further, the angle between two vectors can be determined using the cross product calculation and the arcsine function.

The first Euler angle ϕ is the angle between the $\mathbf{X_1}$-axis and the intersection of the $\mathbf{X_1}$-$\mathbf{Y_1}$ plane of the $\mathbf{X_1}$, $\mathbf{Y_1}$, and $\mathbf{Z_1}$ coordinate system and the x-y plane of the vertebra referenced system. In some preliminary data reduction, the x-y plane of the vertebra coordinate system (inferior body plane) was approximated as containing the y direction vector formed by subtracting the coordinates left edge from the right edge of the inferior body and the x direction vector, formed by subtracting the coordinates of the posterior edge from the anterior edge coordinate of the inferior body. This definition was problematic, because the main bodies of the specimen contained some wedging, not only in the anterior posterior direction but also in the lateral direction. The consequence was that the z axis did not pass through the center of the anterior body plane. To minimize the variability between specimens, the x-y plane was defined by the z axis, which by definition is perpendicular to both the x and y axes. The z direction was determined by subtracting the inferior body center from the superior body center. This definition is also

attractive because the vertebral body is a compressive member, with the force being transmitted by the pressure in the vertebral discs. The superior and inferior forces would be centered within the respective body. The cross product of the z-axis and the normal vector to the $\mathbf{X_1}$-$\mathbf{Y_1}$ plane is perpendicular to both normal vectors and therefore contained in both planes. In other words, the cross product of the normal vectors is in the direction of the intersection of the two planes. The sine of angle ϕ is determined by taking the arcsine of the cross product of a unit vector in the $\mathbf{X_1}$ direction and a unit vector in the direction of the intersection of the $\mathbf{X_1}$-$\mathbf{Y_1}$ plane and the x-y plane.

The data are transformed to the new coordinate system ($\mathbf{X_2}$, $\mathbf{Y_2}$, and $\mathbf{Z_2}$) using the following matrix:

$$\begin{pmatrix} \cos\phi & \sin\phi & 0 \\ -\sin\phi & \cos\phi & 0 \\ 0 & 0 & 1 \end{pmatrix}$$

Note that only the $\mathbf{X_2}$ and $\mathbf{Y_2}$ coordinates are changed from the previous $\mathbf{X_1}$ and $\mathbf{Y_1}$ coordinates, the $\mathbf{Z_2}$ coordinates remain the same as the $\mathbf{Z_1}$ coordinates. That is because the rotation is about the $\mathbf{Z_1}$-axis. Note the sine and cosine functions for the rotation angle ϕ.

The second Euler angle θ is the angle between the $\mathbf{X_2}$-$\mathbf{Y_2}$ plane and the x-y plane. It is also the angle between the normal vector to the $\mathbf{X_2}$-$\mathbf{Y_2}$ plane and the normal vector to the x-y plane. The normal vector to the $\mathbf{X_2}$-$\mathbf{Y_2}$ plane is the $\mathbf{Z_2}$ axis. The normal vector to the x-y plane has to be recalculated because of the rotation, but is still the coordinates of the inferior body center subtracted from the superior body center. Using unit vectors, the cross product of the two normal vectors produces a vector perpendicular to the two

vectors with a magnitude of the sine of the angle between the two vectors. The arcsine of the magnitude of the cross product gives the angle θ.

The data are transformed to the new coordinate system ($\mathbf{X_3}$, $\mathbf{Y_3}$, and $\mathbf{Z_3}$) using the following transformation matrix:

$$\begin{pmatrix} 1 & 0 & 0 \\ 0 & \cos\theta & \sin\theta \\ 0 & -\sin\theta & \cos\theta \end{pmatrix}$$

Angle ψ, the third Euler angle, is the angle between the $\mathbf{X_3}$ axis and the x-axis (or between the$\mathbf{Y_3}$ axis and the y axis). As noted previously, the x-axis is approximated by the vector between the posterior and anterior inferior body of the vertebra and the y-axis is approximated by the vector between the right and left edge of the inferior body of the vertebra. These two definitions however, do not necessarily produce perpendicular vectors. For the purposes of this thesis, angle ψ, is defined as the angle between the$\mathbf{Y_3}$ axis and the y-axis. The y-axis vector is determined using the coordinates of the right and left inferior body measurements and then is made into a unit vector. The cross product of the unit vector in the y direction and the unit vector in the $\mathbf{Y_3}$ direction gives a vector perpendicular to both vectors and of length equal to the sine of the angle between the two vectors (angle ψ). The angle ψ is found using the arcsine function. The data are transformed to the vertebral referenced axis ($\mathbf{X_4}$, $\mathbf{Y_4}$, and $\mathbf{Z_4}$) using the following matrix.

$$\begin{pmatrix} \cos\psi & \sin\psi & 0 \\ -\sin\psi & \cos\psi & 0 \\ 0 & 0 & 1 \end{pmatrix}$$

Finally, a linear translation of the $\mathbf{X_4}$, $\mathbf{Y_4}$, and $\mathbf{Z_4}$ data to the x, y and z axis was required to re-center the origin of the axis system between the left and right and dorsal

and ventral edges of the inferior body plane. Of note, the rotations could have been performed prior to the first translation, avoiding a second translation; however, making the translation first facilitated checking the rotation process by looking at coordinate data. The small change in the center of the vertebra, with respect to the origin of the axis, occurred due to the asymmetry of the vertebrae and the shifting of the data points during the three rotations. This produced the coordinates of the 38 reference points in the vertebral referenced coordinates (x, y, z).

Once the measured coordinates were referenced to the vertebral coordinate system, it was then possible to calculate the unit vectors of interest using very simple calculations:

- The superior-inferior axis vector at the midpoint of the pedicle was calculated by subtracting the inferior coordinates from the superior coordinates.
- The lateral-medial axis vector at the midpoint of the pedicle was calculated by subtracting the medial coordinates from the lateral coordinates.
- The superior-inferior axis vector of the superior facet was calculated by subtracting the inferior coordinates from the superior coordinates.
- The lateral-medial axis vector of superior facet was calculated by subtracting the medial coordinates from the lateral coordinates.
- The superior-inferior axis vector of inferior facet was calculated subtracting the inferior coordinates from the superior coordinates.
- The lateral-medial axis of inferior facet was calculated by subtracting the medial coordinates from the lateral coordinates.
- The normal vector to the superior facet was determined from the cross product of the superior-inferior axis vector of superior facet and the lateral-medial axis vector of superior facet. Recall one of the properties of the cross product calculation is that it can be used to find the vector perpendicular to the plane of two vectors.
- The normal vector to the inferior facet was determined from the cross product of the superior-inferior axis vector of inferior facet and the lateral-medial axis vector

of inferior facet

- The axial direction vector of the pedicle was determined from the cross product of superior-inferior axis vector at the midpoint of pedicle and the lateral-medial axis vector at the midpoint of the pedicle.

The following unit vectors were calculated:

- The major axis of pedicle at its midpoint. This is the vector with the larger magnitude between either the superior-inferior axis vector at the midpoint of the pedicle and the lateral - medial axis vector at the midpoint of the pedicle. The vector was then divided by its length in order to transform it into a unit vector.

- The major axis of the superior facet. This is the vector with the larger magnitude between either the superior-inferior axis vector of the superior facet and the lateral - medial axis vector of the superior facet. The vector was then divided by its length in order to transform it into a unit vector.

- The major axis of inferior facet. This is vector with the larger magnitude between either the superior-inferior axis vector of the inferior facet and the lateral - medial axis vector of the facet. The vector was then divided by its length in order to transform it into a unit vector.

- The unit vector normal to superior facet. This is the vector normal to the center of the superior facet, divided by its length.

- The unit vector normal to inferior facet. This is the vector normal to inferior facet, divided by its length.

- The unit vector in the axial direction of pedicle. This vector describes the axial direction of the pedicle vector, divided by its length.

The vectors calculated via this data transformation were referenced to the vertebra itself. However, this is not necessarily reflective of the vertebra's *in vivo* position. For the purpose of the statistical analysis, it is important to calculate these vectors with respect to the gravity vector as well for comparative information. In this study, an orthograde posture was chosen. This position was chosen as the literature contained some information regarding the vertebral position for this posture.

Radiologically, the lumbosacral junction is well documented in humans. From radiological evidence the angle (ω), the forward rotation of the last lumbar vertebra can be approximated. In this position the human last lumbar vertebra is rotated forward approximately thirty degrees from the horizontal (Yochum and Rowe, 2005). Unfortunately, this angle is not well documented for non-human primates. Therefore, this angle was approximated using indirect evidence. AH Schultz (1961) documented the exact vertebral curvature of the non-human specimens by making molds of the abdominal cavity of eviscerated specimens. His diagrams demonstrate a kyphotic curvature in the thoracic region. However, in lower lumbar region, the diagrams indicate that the spine is held perpendicular to the ground and therefore the last lumbar would not be significantly rotated.

The human coordinate system (x_1, y_1 and z_1) was rotated about the y-axis to the approximate vertebral position with respect to the gravity vector using the following matrix:

$$\begin{pmatrix} \cos\omega & 0 & \sin\omega \\ 0 & 1 & 0 \\ -\sin\omega & 0 & \cos\omega \end{pmatrix}$$

The precision to which landmark points are measured is of great interest. Errors can be induced by the operator (intraoperator error) or by the measuring instrument (instrument error). To minimize the combined intraoperator and instrument error, the landmark points were taken twice on each specimen. While individual points can be compared, the calculated directions are based on several vectors calculated by finding the difference between two measured points. Therefore, the vectors were calculated in real time for both sets of measurements and the direction of the results were compared. In

order to calculate angle error between the vectors found from the two sets of data, the cross product calculation was used. Recall that from the cross product, the sine of the angle between the two vectors can be found. The unit normal vectors calculated from the two sets of data were calculated then the cross product was taken. The angle between the two vectors is the arcsine of the length of the normal vector. This is expressed in radians, which are easily converted to degrees by multiplying the radians by 180 and dividing by pi. The data transformation Excel spread was programmed to calculate this value for six of the unit directionality vectors. The data points were rejected if the angle of difference between the measurements exceeded five degrees. The intraoperator error values were calculated for six of the 12 vectors calculated (Appendix B). The unit vectors were the vectors normal the facets and the vectors axial to the pedicles. These vectors were calculated as they represent the highest errors values possible. Recall that the normal and axial vectors were calculated from four data points and the major axis vectors are calculated from two of the four same landmark points. Please see the Appendix B for a detailed description of the accepted error rates.

CHAPTER 5
STATISTICAL ANALYSIS AND RESULTS

Directional data cannot be analyzed using traditional univariate or multivariate statistics. Fortunately, there are methods available for the analysis of this type of data. To enrich our understanding of the posterior element morphology, both descriptive and comparative statistical methodologies were used to analyze the vector data.

Combining Mixed Sex Samples

Recall from Chapter Three that the species samples are mixed sex. Pooling the males and females of a species increases sample size. However, pooling males and females can be problematic, especially for a species with extreme sexual dimorphism, as this can result in a misleading mean (or Mean Direction) and a large standard deviation (or Mean Resultant Length), making the data insensitive to pair-wise testing. Therefore, before pooling the males and females, it is desirable to determine that they have equal mean directions. However, this is not always possible as was the case with three of the four species included in this project.

The *Pongo pygmaeus* and *Pan troglodytes* samples were composed of specimens of both known and unknown sex. Therefore, it was not possible to determine if the males and females had equal mean directions. When reviewing the results, it is important to keep in mind that these species were pooled without the benefit of the test of equal means.

The test for equal male and female means for the *Homo sapiens* sample was not conducted for a different reason. In the human sample, the sex of each specimen is

known, however, the sample is overwhelmingly male (17 males, 2 females). A statistician was consulted and it was determined that a test to determine if the males and females can be pooled is not meaningful given the extremely small female sample size. However, the reader again is cautioned that if the sample was more balanced, this test would not only be appropriate, it would be required.

Fortunately, the sexes of all specimens are known for the most sexually dimorphic species included in the sample, *Gorilla gorilla*. Further, this sample is fairly balanced. Therefore, the test of equal means direction was conducted.

In order to confidently pool cross-sex specimens, the sex specific samples are required to have not only equal mean direction, but also equal concentration. The equal mean direction hypothesis was tested using corrected version of the Likelihood Ratio Test given in Mardia and Jupp (2000). This corrected test was developed by Presnell and Rumcheva (2005). It is corrected in the sense that instead of referring the test statistic to a chi-square distribution, it is referred an F distribution. This has a better performance in terms of Type I error. The hypothesis of equal mean directions is rejected for large values of the test statistic. The results are reported in the data tables as p-value 1.

Equal concentration was verified using a pair-wise specific test found in Mardia and Jupp (2000). The results are reported in the data tables 5-1 as p-value 2. The null hypotheses of equal mean direction and equal mean concentration were not rejected if the p-value > 0.05.

Table 3 describes the statistical results of the male vs. female gorilla tests. Descriptive statistics, mean direction (MD) and mean resultant length (MRL) are also listed in the table. A detailed description of these values is given in the next section.

Table 3. Pooling data, *Gorilla* sample.

		Superior Facet			
		Left		Right	
		Major Axis	Normal	Major Axis	Normal
Sample Size (M,F)		(9,7)	(-9.7)	(10,7)	(10,7)
Gorilla M	MD	-0.15, 0.67, 0.73	-0.59, -0.66, 0.46	-0.19, -0.75, 0.63	-0.53, 0.69, 0.48
	MRL	0.78	0.95	0.86	0.98
Gorilla F	MD	-0.22, 0.49, 0.84	-0.56, -0.75, 0.36	-0.35, -0.58, 0.74	-0.56, 0.75, 0.36
	MRL	0.86	0.98	0.84	0.98
P-value1		0.6485	0.3721	0.5968	0.1652
P-value2		0.2831	0.0975	0.8084	0.3849
		Inferior Facet			
		Left		Right	
		Major Axis	Normal	Major Axis	Normal
Sample Size (M,F)		(7,7)	(7,7)	(10,7)	(10,7)
Gorilla M	MD	-0.02, 0.18, 0.98	0.58, 0.77, -0.26	0.12, -0.29, 0.95	0.48, -0.80, -0.35
	MRL	0.76	0.97	0.74	0.95
Gorilla F	MD	0.20,0.045, 0.98	0.54,0.81, -0.23	-0.01, -0.43, 0.90	0.52, -0.81, -0.28
	MRL	0.82	0.97	0.74	0.96
P-value1		0.6543	0.7903	0.7874	0.7258
P-value2		0.3222	0.4943	0.5638	0.3223
		Pedicle			
		Left		Right	
		Major Axis	Axial Direction	Major Axis	Axial Direction
Sample Size (M,F)		(8,7)	(8,7)	(10,7)	(10,7)
Gorilla M	MD	0.27, -0.29, 0.92	-0.87, 0.33, 0.38	0.30,0.14,0.94	-0.93, -0.19, 0.32
	MRL	0.99	0.98	0.99	0.97
Gorilla F	MD	0.20, -0.25, 0.95	-0.85, 0.43, 0.31	0.20, 0.21, 0.96	-0.93, -0.28, 0.25
	MRL	0.99	0.97	0.99	0.96
P-value1		0.2864	0.3725	0.122	0.4635
P-value2		0.4241	0.8339	0.4717	0.7506

The results in Table 3 indicate that for all the vectors, male and female gorillas did not reject the null hypotheses of equal mean concentration. The test for equal mean direction indicates that the null hypothesis was not rejected for all the vectors tested. Therefore, the male and female specimens were pooled.

Mean Directions and Mean Resultant Lengths

The descriptive statistics reported in Table 4 give information regarding mean values and the variability about that mean. In the case of directional data, the statistical data is expressed as mean direction (MD) and mean resultant length (MRL). The mean direction (MD) is a unit vector, resulting from the means of the x, y, and z coordinates. These values are divided by the mean resultant length (MRL) so that the vector becomes a unit vector. The mean resultant length (MRL) is a measure of concentration that is analogous to a standard deviation. The mean resultant length is obtained by applying Pythagorean Theorem (length = square root of the sum of the squares of the three mean values) to the mean direction vector, prior to its conversion to a unit vector. Descriptive statistics are given for all four species of the sample.

The first goal of this project is to test the feasibility of the development of species-specific vector based models for calculating force magnitude in the posterior vertebral elements. In order to develop such a model, there must be tolerable within-species diversity with respect to the axial and normal vectors calculated. The mean directions (MD) and mean resultant lengths (MRL) for each species are listed in the tables below. The major axis vectors, while not calculated for the first goal of this project, were included.

Table 4. Descriptive statistics.

Superior Facet					
		Left		Right	
Vector		Major Axis	Normal	Major Axis	Normal
Sample Size		(19,16,18,5)	(19,16,18,5)	(16,17,18,5)	(16,17,18,5)
Homo	MD	-0.36,0.77,0.52	-0.62, -0.62,0.48	-0.43, -0.77,0.47	-0.56,0.64,0.53
	MRL	0.84	0.97	0.89	0.98
Gorilla	MD	-0.18,0.59,0.79	-0.58, -0.70,0.42	-0.33, -0.67,0.67	-0.55,0.72,0.43
	MRL	0.82	0.96	0.86	0.98

Table 4. Continued

Superior Facet					
		Left		Right	
Vector		Major Axis	Normal	Major Axis	Normal
Sample Size		(19,16,18,5)	(19,16,18,5)	(16,17,18,5)	(16,17,18,5)
Pan	MD	-0.14,0.43,0.89	-0.45, -0.83,0.34	0.08, -0.33,0.94	-0.34,0.88,0.33
	MRL	0.84	0.99	0.95	0.99
Pongo	MD	0.35,0.31,0.89	-0.64, -0.61,0.46	0.25, -0.59,0.77	-0.72,0.45,0.54
	MRL	0.97	0.96	0.94	0.97
Inferior Facet					
		Left		Right	
Vector		Major Axis	Normal	Major Axis	Normal
Sample Size		(19,14,18,5)	(19,14,18,5)	(19,17,18,5)	(19,17,18,5)
Homo	MD	0.85, -0.21,0.49	0.51,0.69, -0.50	0.83,0.03,0.55	0.47, -0.71, -0.52
	MRL	0.67	0.98	0.58	0.98
Gorilla	MD	0.09,0.11,0.99	0.56,0.79, -0.24	0.07, -0.35,0.93	0.49, -0.81, -0.32
	MRL	0.78	0.97	0.74	0.96
Pan	MD	0.53,0.02,0.85	0.39,0.89, -0.25	0.54, -0.07,0.84	0.31, -0.92, -0.25
	MRL	0.90	0.99	0.92	0.99
Pongo	MD	0.56,0.15,0.81	0.51,0.70, -0.49	0.48, -0.25,0.84	0.63, -0.56, -0.54
	MRL	0.99	0.98	0.99	0.96
Pedicle					
		Left		Right	
Vector		Major Axis	Axial Direction	Major Axis	Axial Direction
Sample Size		(17,15,18,2)	(17,15,18,2)	(17,17,18,4)	(17,17,18,4)
Homo	MD	0.51,0.84, -0.20	-0.76,0.55,0.36	0.56, -0.82,0.15	-0.83, -0.48,0.28
	MRL	0.82	0.98	0.56	0.98
Gorilla	MD	0.24, -0.27,0.93	-0.86,0.37,0.35	0.26,0.17,0.95	-0.93, -0.23,0.29
		0.99	0.97	0.98	0.97
Pan	MD	0.37, -0.28,0.88	-0.80,0.39,0.46	0.38,0.18,0.91	-0.86, -0.29,0.42
	MRL	0.99	0.99	0.99	0.99
Pongo	MD	0.61,0.59,0.53	-0.80,0.53,0.29	0.27, -0.15,0.95	-0.89, -0.35,0.30
	MRL	0.57	0.99	0.69	0.98

The descriptive statistics, MD and MRL values, are given in Table 4. With respect to the superior facet vectors, the left major axis vectors indicate relatively low concentration for *Homo, Gorilla*, and *Pan* while the *Pongo* vectors have high concentrations. Interestingly, for the right major axis vectors, *Homo* and *Gorilla* have

low concentrations while *Pan* and *Pongo* have high concentrations. For the left and right normal vectors, all species have high concentration values.

The results for the inferior facet vectors indicate that for the left and right major axis vectors, *Homo* and *Gorilla* have low concentrations. The *Pan* and *Pongo* major axis vectors have high concentration. The left and right normal vector data for all species indicates very high concentration values.

For the pedicles, the descriptive statistics that the left and right major axis vectors have low concentrations for *Homo* and *Pongo.* The MRL values for *Gorilla* and *Pan* indicate that these vectors have a high concentration. The right and left normal vectors have high MRL values for all four species. Interestingly, only humans have low concentration for all the pedicle major axis vectors.

It is interesting to note that for the superior and inferior facet major axis vectors, the chimpanzee and orangutan vectors have high concentrations. Comparatively, humans and gorillas have relatively low concentrations.

Pair-wise Testing

Pair-wise tests were conducted in lieu of an ANOVA. Preliminary testing indicated that pair-wise testing was a more appropriate for determining mean directional differences. These preliminary tests demonstrated that it was likely that all species had statistically different mean values. Therefore, four-way ANOVA testing would not give results with a satisfactory level of detail.

Further the preliminary testing indicated that for the between-species pair-wise testing, a test that assumes equal concentration was not appropriate. A test that does not assume equal concentration, also based upon the von Mises-Fisher distribution (Mardia and Jupp 2000), was performed. A total of 60 pair-wise tests were conducted. The

orangutan data were not included in the pair-wise tests as the sample size was quite small (n=2-5) and the results would not be meaningful. Pair-wise tests were conducted with both the vertebral referenced system and the data rotated to account for the in-vivo gravity vector.

Tables 5 lists the results for the pair-wise analyses for the superior facet, inferior facet, and pedicle vectors. The null hypothesis of equal mean direction was not rejected for p-values <0.05. Five pair-wise tests were conducted for each sample, *Gorilla* vs. unrotated *Homo*, Gorilla vs. rotated *Homo, Gorilla* vs. *Pan, Pan* vs. unrotated *Homo*, and *Pan* vs. rotated *Homo.*

Table 5. Pair-wise results.

Test of Equal Mean Direction,				
Superior Facet Vectors				
	Left			
	Major Axis	Normal	Major Axis	Normal
Gorilla vs. *Homo* (Sample Size)	(16,19)	(16,19)	(17,16)	(17,16)
p-value	0.0570	0.2074	0.1866	0.0708
Gorilla vs. Rotated *Homo*	(16,19)	(16,19)	(17,16)	(17,16)
p-value	0.2099	<0.0001	0.2398	<0.0001
Gorilla vs. *Pan*	(16,18)	(16,18)	(17,18)	(17,18)
p-value	0.4338	0.0026	<0.0001	<0.0001
Pan vs. *Homo*	(18,19)	(18,19)	(18,16)	(18,16)
p-value	0.0005	<0.0001	<0.0001	<0.0001
Pan vs. Rotated *Homo*	(18,19)	(18,19)	(18,16)	(18,16)
p-value	0.0089	<0.0001	<0.0001	<0.0001
Inferior Facet Vectors				
	Left		Right	
	Major Axis	Normal	Major Axis	Normal
Gorilla vs. *Homo* (Sample Size)	(14,19)	(14,19)	(17,19)	(17,19)
p-value	<0.0001	<0.0001	0.0004	0.0015
Gorilla vs. Rotated *Homo*	(14,19)	(14,19)	(17,19)	(17,19)
p-value	<0.0001	<0.0001	<0.0001	<0.0001
Gorilla vs. *Pan*	(14,18)	(14,18)	(17,18)	(17,18)
p-value	0.0139	0.0017	0.0022	0.0005

Table 5. Continued

Test for Equal Mean Direction				
Inferior Facet Vectors				
	Left		Right	
	Major Axis	Normal	Major Axis	Normal
Pan vs. *Homo (Sample Size)*	(18,19)	(18,19)	(18,19)	(18,19)
p-value	0.0125	<0.0001	0.1306	<0.0001
Pan vs. Rotated *Homo*	(18,19)	(18,19)	(18,19)	(18,19)
p-value	<0.0001	<0.0001	<0.0001	<0.0001
Pedicle Vectors				
	Left		Right	
	Major Axis	Axial	Major Axis	Axial
Gorilla vs. *Homo*	(15,17)	(15,17)	(17,17)	(17,17)
p-value	<0.0001	<0.0001	<0.0001	<0.0001
Gorilla vs. Rotated *Homo*	(15,17)	(15,17)	(17,17)	(17,17)
p-value	<0.0001	0.0011	*<0.0001*	<0.0001
Gorilla vs. *Pan* (Sample Size)	(15,18)	(15,18)	(17,18)	(17,18)
p-value	0.0005	<0.0001	0.0013	0.0093
Pan vs. *Homo*	(18,17)	(18,17)	(18,17)	(18,17)
p-value	<0.0001	<0.0001	<0.0001	<0.0001
Pan vs. Rotated *Homo*	(18,17)	(18,17)	(18,17)	(18,17)
p-value	<0.0001	<0.0001	<0.0001	<0.0001

With respect to the superior facet vectors, the vectors generally have statistically different mean directions. There are exceptions. The *Gorilla* vs. unrotated *Homo* test indicates that the right and left major axis and normal vectors do not have statistically different mean directions (p-values, 0.0570, 0.2074, 0.1866, and 0.0708 respectively). The pair-wise tests for *Gorilla* and rotated *Homo* indicate that the right and left superior facet major axis vectors do not have statistically different mean directions (p-values 0.2099 and 0.2398 respectively). Finally, the *Gorilla* vs. *Pan* pair-wise tests indicate that for the left superior facet major axis vector they do not have statistically different mean directions (p-value 0.4338).

For the inferior facet vectors, all tests except one indicate that each species has statistically different mean directions. The exception is the *Pan* vs. unrotated *Homo* right inferior facet major axis vector test. The pair-wise test indicated that for this vector, humans and chimpanzees do not have statistically different mean directions.

With respect to the pedicle vectors, the results indicate that the species have statistically different mean directions ($p<0.05$).

CHAPTER 6
DISCUSSION

Pair-wise Testing

An overwhelming majority of pair-wise tests indicate the each species vector had a statistically different mean direction. However, a minority of the pair-wise tests indicated did not reject the null hypothesis. With respect to the *Homo* and *Gorilla* pair-wise tests, the superior facet vector results indicated that when the human vectors were not rotated to the gravity vector, the right and left major axis and normal vectors did not have statistically different mean directions. This would suggest that, with respect the major axis vectors, *Homo* and *Gorilla* species have a similar direction of motion for the superior facets. The equal mean normal vectors indicate that *Homo* and *Gorilla* have a similar pattern of force transmission in the superior facets. However, these results are problematic; when the human spine is held vertically to the ground, the last lumbar is rotated forward 30 degrees from the horizontal. When the same pair-wise test was conducted with the rotated *Homo* vectors, the major axis vectors indicate equal mean directions with an even higher p-value (p-value 0.0570 and 0.1866 vs. 0.2099 and 0.2398). However, the normal vectors no longer have equal mean directions (MD), suggesting they have different force transmission patterns in the superior facets. These results are difficult to interpret. It would seem to indicate that despite a dramatic change in human vectors orientation, humans and gorillas have statistically non-divergent superior facet major axis orientation, which in turn may suggest that the superior facets allow the greatest rotation in the same plane. However, the functional interpretation of

this is not yet clear. More research, such as the calculation of facet curvature, is necessary to prove the assumption that the major axis facet vectors have a functional significance.

The *Pan* vs. *Gorilla* pair-wise tests indicate that for the left superior facet major axis vectors, they do not have statistically different mean directions. It is surprising that the right major axis vector does not indicate an equal mean direction as well, (p-values 0.4338 and <0.0001 respectively). Interestingly, this asymmetrical pattern is echoed in the pair-wise results for the inferior facet major axis vectors of *Pan* and unrotated *Homo* vectors. However, the side is reversed. In this case the left major vectors indicate that they do not have equal mean directions, while the right indicate equal mean direction, (p-values of 0.0125 and 0.1306 respectively). The assumption that these vectors are measuring function has not been proven. These results may indicate that they are not accurately capturing function as intended. These asymmetrical results may also be the result of Type I error.

Pair-wise Comparisons and Phylogeny

The pair-wise tests were conducted in three closely related species, humans, chimpanzees, and gorillas. The phylogenetic relationship between these species is still contested. However, molecular (Koop et al., 1989; Ruvolo, 1997; Satta et al., 2000 Salem et al., 2003), morphological (Begun, 1992; Shoshani et al., 1996), and morphometric (Lockwood et al., 2004) studies suggest that humans and chimpanzees are more closely related to each other than either is to gorillas. If unit vector orientation was dependent upon phylogenetic constraint one would expect that one of two outcomes: all species would have statistically non-divergent mean directions or alternatively humans and chimpanzees would have statistically non-divergent mean direction, while gorillas

would have statistically different mean directions. However, the results indicate, overwhelmingly, that each species has statistically different mean values for the vectors calculated, suggesting that facet and pedicle orientation are not a consequence of phylogenetic constraint.

Pair-wise Comparisons and Allometry

In order to address allometry, the sample included males and females of a highly dimorphic species (*Gorilla gorilla*) as well as two species that have similar body size (*Homo sapiens* and *Pan troglodytes*). The *Gorilla* test for equal means for males and females indicate that the vectors calculated have a small dispersal and statistically non-divergent mean directions. The *Homo sapiens* and *Pan troglodytes* pair-wise tests indicate that despite a similarity in body size, these vectors are statistically different between the species. While this is not conclusive, the results suggest that these vectors are insensitive to body size alone.

Pair-wise Comparisons and Bone Biology and Behavior

To investigate whether bone size and shape are indicative of load transmission, it is necessary to calculate the forces that these elements are subject to during normal loading. To better understand the force data, when it is obtained, pair-wise analyses were conducted for the "force" vectors.

When considered with respect to a biomechanical model, three vectors in the analysis may be indicative of force transmission patterns. They are the pedicle major axis and axial vectors as well as the vectors that are normal to the superior and inferior facets.

A simplified two-dimensional free body diagram indicates that the mean normal and axial vectors can be used as a starting point for developing models for force

calculation in the posterior elements. The pair-wise comparison results indicate that for all of these vectors, each species has a statistically different mean direction. This would suggest that each species does in fact have different force transmission patterns in the posterior elements. It is somewhat surprising that the gorilla and chimpanzee vectors are statistically different as the most frequently engaged locomotor behavior for both species is knuckle-walking. However, it is not totally surprising, as ANOVA tests from Shapiro (1991,1993) demonstrated statistically different mean values for the parameters she measured. Perhaps these data indicate that facet and pedicle orientation is responsive to the species' total locomotor/postural repertoire, not simply orthograde posture or the most frequently engaged in locomotion. Further, the descriptive statistics indicate the vectors had very high concentrations. This may suggest that facet and pedicle orientation is highly constrained. Current, there have been no research studies to determine the extent of morphological canalization of the primate spine. Clearly, this research is a necessary component to a function morphological analysis of the spine as it gives important information with respect to extent that development and function affect morphology.

The pedicle major axis vector may also be an important indicator of force transmission patterns. The pedicles connect two compressive columns and they are assumed to be involved in force transmission and subject to stresses and strains. The mechanism of force transmission through the pedicles is not understood and consequently the nature of the stresses and strains are not understood. However, it has been suggested that one possibility is that the pedicle is being subjected to bending stresses. The long, or major axis, of the pedicle has the ability to resist the most bending force. As would be

expected from the facet normal and pedicle axial results, the pair-wise tests indicate that each species has a statistically different mean direction with respect to this vector.

Of note, the descriptive statistics demonstrate that *Gorilla* and *Pan* mean pedicle major axis vectors have high concentration values. However, the human pedicle major axis vectors have very low concentrations indicating that humans lack the uniformity of major axis direction that was found for the non-human primates. As the exact mechanism of force transmission is not currently known, it is not clear whether this measure has functional significance. The work of Shapiro (1991; 1993) and Sanders (1995; 1998) both demonstrated that human pedicles, especially at the last lumbar are short and wide. In humans, the minor axes-major axes ratio data for the pedicles (Appendix A) indicate that there is a general trend for lateral and superior axes to be of fairly similar in length. This would indicate that, in cross section, human pedicles may be more accurately described as round, rather than elliptical. This would make defining the major axis more difficult may explain the low concentration values. More calculation of forces acting upon the pedicle is necessary to determine if it is subjected to significant bending forces.

Force Transmission in the Posterior Elements

The exact manner of force transmission with individual posterior elements is not clearly understood. The most current model, the two column model of force transmission, states that the vertebral bodies and disks form one compressive column, while the posterior elements comprise a second compressive column. The pedicles are a bony bridge between the two columns. It has been hypothesized that the pedicles are subjected to significant bending stresses as a result of muscles action on the spinous or transverse processes or alternately from the posterior elements (Bogduk and Twomey,

1987). Alternately, Bogduk and Twomey also suggested that the pedicles may be subjected to tension from the facets locking to prevent the vertebrae from sliding forward (Bogduk and Twomey, 1987). It has also been hypothesized that the pedicles may be subjected to compressive axial loads from the vertebral body to the lamina (Pal and Routal, 1986, 1987). There are four potential forces acting in the pedicle, torsion, compression, bending and shear. The development of a biomechanical model of the pedicles and posterior elements will help determine the extent to which these forces are significant.

Sanders (1998) also hypothesized that facet spacing is important for the resistance of compressive force in the posterior elements. He suggested that the more widely spaced facets that he demonstrated in humans may create a more stable base. Intuitively this hypothesis is satisfactory. However, the development of an accurate biomechanical model is necessary to prove if this is a correct interpretation of this aspect of posterior element morphology.

Feasibility of the Model

With respect to the development of species models for the calculation of stresses, the results are very encouraging. The vectors necessary for the current simplified model, normal and axial, all have very high mean resultant lengths. However, the model does not incorporate the effects of muscle attachments and the subsequent stresses and strains caused by muscle action. It should be possible to calculate that loads borne by the lumbar spine, if the muscle forces can be accurately modeled and the position of the vertebrae during diverse locomotor behavior is known. More research is needed document the angles of the vertebra with respect to the gravity vector or alternately a methodology needs to be developed that can estimate these angles. This research may

include estimation from radiographic information or possibly estimating the angles using known biological parameters (arm, leg, and trunk length, weight, and documented positional and locomotor behavior). However, it would be necessary to develop a measure of accuracy for such estimations.

Vector Concentrations (MRL)

The concentration values (MRLs) are extremely important measures of within sample variability. The measure of concentration (MRL) is a number from 0-1. A value of one indicates that the vectors are parallel and a value of zero indicates that the vectors are randomly oriented. When interpreting the validity of a mean value, it is necessary to have an approximate cut-off value of for concentration. The cut off value is subjective, and varies from project to project. However, if we had a sample of ten vectors and five had an equal lateral mean direction and five had equal mean directions perpendicular to the lateral vectors, the concentration (MRL) value would be ~0.70. For the purpose of building the current project a high degree of precision is required and the values were considered to have high concentration for values of ~0.95 and above.

Facet Shape

This research indicates that the species included in the sample have 5 major facet shape types as outlined in Figure 8. Thus far, no other study has addressed the issue of facet shape. It is important to note that these facet types were defined qualitatively, in the interest of having a consistent major axis, and by default, minor axis designations for each shape. It is not clear, based on this research, if these shapes are exclusive or if they correlate with other factors. More work is necessary to quantitatively document facet shape including facet curvature, which may lead to an understanding of correlation with other factors. Further it has been hypothesized that the facet major axis vectors may

indicate a preferred direction of motion. Analysis of facet curvature will give additional information as to whether this measure is a reasonable approximation of the direction of facet rotation. A Fourier analysis would be appropriate for this study as orientation is an important factor.

CHAPTER 7
CONCLUSIONS

The results of this study further confirm that the lumbar spine, specifically the last lumbar vertebra, is fertile ground for future functional morphological studies. The morphology of the spinal column is critical to postural and locomotor behavior. One important goal in a functional morphological analysis on the spine is to determine if there is a relationship between the size and shape of a bony element and the loads it must withstand. The current research indicates that generalized species models can be developed. The vectors that are key to the development of these models, normal and axial, were demonstrated to have high concentrations and therefore can form the basis for valid models for each species. Further, these high concentration values may indicate that this measure of facet and pedicle orientation is not sensitive to individual behavior. Rather, the orientation is very consistent within species. Pair-wise tests indicate that the human, gorillas, and chimpanzees have unique mean directions for these vectors, with the exception of the unrotated human and gorilla. This test demonstrated that these species have statistically equal mean directions.

Previously undocumented vertebral measures, the major axes of the facets and pedicles, were also addressed. The facets joints allow, or alternatively constrict, motion within the spinal column. The direction of this vector may indicate the plane in which the facet allows the most rotation. The statistical analyses overwhelmingly indicate that humans, gorilla and chimpanzees have unique mean directions with respect to these vectors. There were a few exceptions. For both the unrotated and rotated human vectors

and gorilla vectors, pair-wise tests indicate these two species have statistically non-divergent mean directions. Another exception was the left superior facet major axis vectors of gorilla and chimpanzees. The left, though notably not the right, vectors of these species have non-divergent mean directions. Finally, the unrotated human and chimpanzee pair-wise test of the right inferior major axis vectors, though not the left, indicate that these two species have statistically non-divergent mean directions. The functional implications of these data are not readily transparent.

Interestingly, the results of the major axis facet analyses demonstrate a low concentration of the facet major axes vectors. The low concentrations indicate within species variability for this measure. This seems to suggest that facet shape is responsive and plastic in the individual, though it is not clear if it is responsive to locomotor and postural behaviors.

The pedicle major axis vectors were measured, as this directional vector may indicate how the pedicle is oriented to resist the most bending force. Results of the statistical analyses of pedicle major axis vectors are also very interesting in that they indicate the species have statistically different mean directions with respect to this measure. Finally, with regard to concentration, gorillas and chimpanzees have extremely high concentrations. However, human major axis pedicle vectors have extremely low concentration values. These results may indicate that the major axis vector is not measuring function as intended. The minor-axis major axis ratio calculation (Appendix A) confirms that there is a general trend in humans for the medial and lateral axes to be fairly equal in length. Further, the shape of the pedicle may not be ideally suited, as is assumed, to a specific type of force. The trend in orthograde primates to have short, wide

pedicles may indicate that the response to increased compressive loads is constrained by function or neurological considerations. Finally, the results of this analysis demonstrate that, given certain assumptions, it is possible to develop species-specific models to calculate forces in the spinal column.

APPENDIX A
MAJOR AXES-MINOR AXIS RATIO

The tables below list the major axis-minor axis ratio for each specimen. The value is calculated via the formula log (superior-inferior axis) - log(lateral-medial axis). This value is the base ten logarithm of the ratio of the major to minor axis. A positive value indicated that the superior-inferior axis is longer, while a negative value indicated that the lateral-medial axis is the longer of the two axes.

Homo major axis-minor axis ratio.

Homo	Right Pedicle	Left Pedicle	Right Sup. Facet	Left Sup. Facet	Right Inf. Facet	Left Inf. Facet
1	0.154004028	0.122777501	-0.076485421	-0.083315591	-0.036990687	0.085841076
2	-0.168245483	-0.024223181	-0.034702602	0.045502107	-0.035288941	0.200988587
3	-0.022722562	-0.003593294	-0.10217809	-0.137450031	0.133044418	0.143808298
4	NA	NA	0.191864849	-0.181905303	0.108410102	0.144166515
5	-0.19587025	-0.008572706	-0.099681284	-0.10488135	0.139241109	0.19679049
6	-0.008060033	-0.049878814	0.189004265	0.090310548	0.136960776	-0.073634987
7	-0.205698218	-0.120912741	-0.176895834	-0.059726442	-0.111932747	-0.115985709
8	0.011222033	0.029822045	-0.083507239	-0.047776674	0.211911927	0.006849671
9	0.165669964	-0.017378339	-0.061136929	0.066483798	0.209886421	0.234550164
10	-0.14308604	-0.148556922	-0.029226677	-0.16739032	0.115877559	0.222156199
11	-0.023937285	-0.108195036	-0.019557449	-0.150507035	0.14289058	0.162482517
12	0.021455712	-0.01708491	-0.048078851	-0.047295453	-0.120152347	-0.13369963
13	NA	NA	-0.054751394	-0.062539143	0.111309967	0.31360054
14	-0.153090849	-0.18451456	-0.009755018	-0.013468729	0.036861323	0.105409743
15	-0.157696731	-0.1701001	NA	-9.11852E-05	0.05109364	-0.058043173
16	-0.093144815	-0.124482014	-0.183166616	-0.162388367	-0.194479701	0.02441287
17	> 0.001	-0.065732342	NA	-0.228174563	0.118806321	0.076225337
18	0.017244966	-0.03146184	0.064152452	0.081666506	0.209628657	0.078556068
19	0.038259755	-0.047534837	NA	-0.078808292	0.073729481	0.082819371

Gorilla major axis-minor axis ratio.

Gorilla	Right Pedicle	Left Pedicle	Right Sup. Facet	Left Sup. Facet	Right Inf. Facet	Left Inf. Facet
1	0.060167877	0.067643681	-0.064164788	-0.217178634	-0.222365457	0.038108348
2	0.127629537	0.223340381	0.130056818	0.218542269	0.056772197	0.112606279
3	0.375613123	0.320078963	-0.357718716	-0.182414896	-0.114841461	0.043987822
4	0.222651315	0.246796519	0.256098669	0.145279049	0.167937031	0.159292774
5	0.287470785	0.182472506	0.138466694	0.121439514	-0.003561981	0.081388742

Gorilla. Continued.

Gorilla	Right Pedicle	Left Pedicle	Right Sup. Facet	Left Sup. Facet	Right Inf. Facet	Left Inf. Facet
6	0.12936712	0.145883044	-0.084745501	-0.039511551	0.074280664	0.120548935
7	0.141641702	0.222122531	-0.127360023	-0.134062605	0.026483505	NA
8	0.081080411	0.119080867	-0.192925955	-0.27067006	0.081999694	-0.082457784
9	0.119551448	0.164047131	0.251696202	-0.226917138	-0.159622372	-0.204039531
10	0.137548209	NA	0.224990253	0.079112759	0.321164729	0.26279744
11	0.101727584	0.148862339	-0.121686273	-0.146663289	0.047584429	-0.02817221
12	0.118749878	0.084090499	-0.131024216	-0.137255376	-0.158394163	-0.09308975
13	0.138983315	NA	0.165514375	NA	0.123303367	NA
14	0.137558074	0.223620517	-0.088671365	0.08403637	-0.227318767	0.190659229
15	0.134192423	0.086933583	-0.124312935	0.136050062	0.03654971	0.067166727
16	0.300352283	0.216250665	-0.203508887	-0.010258393	0.029210435	NA
17	0.248338172	0.176788136	-0.147019214	-0.060164388	0.166190544	0.058113367

Pan minor axes-major axes ratio.

Pan	Right Pedicle	Left Pedicle	Right Sup. Facet	Left Sup. Facet	Right Inf. Facet	Left Inf. Facet
1	0.22183874	0.280385713	0.131302338	0.141002239	0.144568675	0.106252181
2	0.255433552	0.200764578	0.124194868	0.102431458	0.061718878	0.165303483
3	0.405821594	0.341866563	0.155701514	0.154558942	0.057895504	0.145964859
4	0.326159647	0.281167648	0.039289209	-0.091357267	0.194611474	0.283394472
5	0.259558909	0.212682574	0.085998391	-0.024546424	0.219947716	0.231392834
6	0.106969764	0.103704398	0.110323302	0.217555913	0.000779009	-0.044905124
7	0.18342086	0.199781293	0.154620771	0.121204753	0.154995693	0.281804273
8	0.253017076	0.262167926	-0.016198363	-0.036284862	0.208380764	0.199520161
9	0.28797178	0.189091318	0.15263867	0.090480153	0.040798182	-0.162966207
10	0.184171769	0.252979075	0.10504127	0.038045831	0.013012161	0.047561334
11	0.084186624	0.171771641	0.063849173	-0.136923196	0.111160804	0.023174003
12	0.383823739	0.345946783	0.097182104	0.096102229	-0.088161714	0.049324453
13	0.277177855	0.259971814	0.190514199	0.072523392	0.17743898	0.061610458
14	0.151779711	0.192508569	0.086232445	0.033836483	0.189028532	0.215425648
15	0.210597829	0.210260155	0.14357679	0.10951732	0.18732476	0.141981253
16	0.321865888	0.317752038	0.122224054	0.146863685	0.27884123	0.166475019
17	0.257802873	0.222618699	0.052256937	-0.09097867	0.131903682	0.161802253
18	0.272826335	0.307301703	-0.080063049	-0.049644983	0.110340009	0.143839923

Pongo minor axes-major axes ratio.

Pongo	Right Pedicle	Left Pedicle	Right Sup. Facet	Left Sup. Facet	Right Inf. Facet	Left Inf. Facet
1	0.092599566	NA	0.062045738	0.027134765	0.06229625	0.151568419
2	-1.382393424	-1.354590371	0.070912757	0.02605175	0.100561634	0.18084306
3	0.381737882	-1.195793895	0.211296274	0.241418164	0.162105728	0.044230445
4	-0.062836729	-0.048311536	0.30678293	0.266221028	0.173352109	0.200495819
5	0.135336062	0.252095092	0.234525199	0.104844507	0.161262349	0.323901507

APPENDIX B
ANGLE ERROR CALCULATION (DEGREES)

Homo.

Angle Error Calculations	Mean	Std. dev.	n=
Normal to Superior Facet Right	1.38239	0.882528	16
Normal to Superior Facet Left	1.694435	0.677398	19
Normal to Inferior Facet Right	1.503308	0.777949	19
Normal to Inferior Facet Left	1.369888	0.788105	19
Axial Direction of Pedicle Right	2.326571	1.198554	17
Axial Direction of Pedicle Left	2.047828	1.010862	17
All	1.712785	0.944116	107

Gorilla.

Angle Error Calculations	Mean	Std. dev.	n=
Normal to Superior Facet Right	1.517525	0.886495	17
Normal to Superior Facet Left	2.195902	1.407393	16
Normal to Inferior Facet Right	2.579414	1.632107	17
Normal to Inferior Facet Left	1.768057	1.152024	14
Axial Direction of Pedicle Right	2.368777	1.098082	17
Axial Direction of Pedicle Left	1.664009	0.992631	15
All	2.028797	1.257412	96

Pan.

Angle Error Calculations	Mean	Std. dev.	n=
Normal to Superior Facet Right	1.496232	1.033072	18
Normal to Superior Facet Left	2.067263	0.978035	18
Normal to Inferior Facet Right	1.666827	1.058175	18
Normal to Inferior Facet Left	3.829464	1.758387	18
Axial Direction of Pedicle Right	1.939254	0.585871	18
Axial Direction of Pedicle Left	2.229736	0.786581	18
All	1.879014	0.973882	108

Pongo.

Angle Error Calculations	mean	Std. dev.	n=
Normal to Superior Facet Right	1.258144	0.407892	5
Normal to Superior Facet Left	1.676243	0.662998	5
Normal to Inferior Facet Right	2.905199	1.387219	5
Normal to Inferior Facet Left	2.034397	0.886031	5

Pongo. Continued

Pongo pygmaeus Angle Error Calculations	mean	Std. dev.	n=
Axial Direction of Pedicle Right	1.437808	1.166763	5
Axial Direction of Pedicle Left	1.507351	0.693615	4
All	1.813392	1.018929	29

APPENDIX C
RAW VECTOR DATA TABLES

Tables 8-1 through 8-4 contain the raw vector data.

Key:
A. = axial
AMNH#-American Museum of Natural History Inventory Number
Dir. = direction
Inf. = inferior
L. = left
MA = major axis
N. = normal
Ped.= pedicle
R. = right
Sup. = superior
Yo = years old

Homo.

Raw Vector Data									
	AMNH# 98-46, 82 yo, Wt. Male			AMNH# 98.49, 74yo, Wt. Male			AMNH# 98-52, 60yo, Wt. Male		
Description of Vector	x	y	z	x	y	z	x	y	z
MA of Ped. R.	0.217647	0.25191	0.94296	0.31027	-0.7929	-0.52448	0.40255	-0.85729	-0.32095
MA of Ped. L.	0.139378	-0.3266	0.93484	0.49412	0.78444	-0.37484	0.37423	0.81527	-0.44191
MA of Sup. Facet R.	-0.485039	-0.8393	0.24558	-0.5126	-0.7847	0.34858	-0.67793	-0.66194	0.31977
MA of Sup. Facet L.	-0.485757	0.78904	0.37611	0.39183	0.55654	0.73262	-0.53428	0.68735	0.49202
MA of Inf. Facet R.	-0.117477	-0.7618	0.63709	-0.21229	-0.8701	0.44491	0.79758	0.08984	0.59648
MA of Inf. Facet L.	0.874694	-0.1862	0.44749	0.71831	-0.6354	0.28338	0.89112	-0.17631	0.41812
N. to Sup. Facet R.	-0.67373	0.53768	0.50694	-0.65182	0.61989	0.43688	-0.51864	0.73894	0.43009
N. to Sup. Facet L.	-0.587696	-0.6133	0.52768	-0.81089	-0.1673	0.56077	-0.47226	-0.72547	0.50066
N. to Inf. Facet R.	0.401513	-0.6232	-0.67113	0.6214	-0.4716	-0.62569	0.44479	-0.75555	-0.48095
N. to Inf. Facet L.	0.456574	0.62634	-0.63185	0.59404	0.34813	-0.7252	0.38613	0.77864	-0.4946
A. Dir. Of Ped. R.	-0.909646	-0.2979	0.28953	-0.80119	-0.5151	0.30466	-0.87403	-0.46417	0.14361
A. Dir. Of Ped. L.	-0.864222	0.42075	0.27584	-0.62879	0.62019	0.46903	-0.88839	0.45184	0.08125
	AMNH# 98-102, 67yo, Wt. Male			AMNH# 98-119, 44yo, Wt. Male			AMNH# 98-125, 50yo, Wt. Male		
Description of Vector	x	y	z	x	y	z	x	y	z
MA of Ped. R.	0.34507	-0.8814	-0.32258	0.38664	-0.8305	-0.40099	0.45885	-0.76618	-0.4499
MA of Ped. L.	0.594566	0.78605	-0.16917	0.51345	0.77332	-0.37196	0.53888	0.78943	-0.29395
MA of Sup. Facet R.	-0.405535	-0.7452	0.52939	0.18703	-0.4657	0.86498	-0.62033	-0.70966	0.33402
MA of Sup. Facet L.	-0.367225	0.72564	0.58188	-0.07188	0.51237	0.85575	-0.58076	0.75949	0.29307
MA of Inf. Facet R.	0.984399	0.16947	0.04731	0.76035	0.05166	0.64745	-0.71522	-0.56723	0.4083
MA of Inf. Facet L.	0.898105	-0.4298	0.09324	-0.54579	0.7152	0.43658	-0.49445	0.75331	0.43364
N. to Sup. Facet R.	-0.591147	0.65554	0.46991	-0.60849	0.63634	0.47414	-0.56898	0.70028	0.43113

Homo. Continued

Raw Vector Data									
	AMNH# 98-102, 67yo, Wt. Male			AMNH# 98-119, 44yo, Wt. Male			AMNH# 98-125, 50yo, Wt. Male		
Description of Vector	x	y	z	x	y	z	x	y	z
N. to Sup. Facet L.	-0.486314	-0.6831	0.54491	-0.44223	-0.7854	0.4331	-0.64243	-0.64869	0.40801
N. to Inf. Facet R.	0.175937	-0.9451	-0.27526	0.4765	-0.7218	-0.50199	0.41403	-0.81454	-0.40634
N. to Inf. Facet L.	0.432632	0.82535	-0.36281	0.55787	0.69892	-0.44754	0.57304	0.65763	-0.48903
A. Dir. Of Ped. R.	-0.694192	-0.471	0.54431	-0.85747	-0.4838	0.17519	-0.75952	-0.601	0.24886
A. Dir. Of Ped. L	-0.673776	0.6019	0.42865	-0.68503	0.63044	0.36508	-0.70487	0.61364	0.35582
	AMNH# 98-59, 70yo, Wt. Male			AMNH# 98-135, 52yo, Wt. Male			AMNH#, 98-147, 50yo, Wt. Male		
Description of Vector	x	y	z	x	y	z	x	y	z
MA of Ped. R.	0.04487	0.20633	0.97745	-0.03115	0.20715	0.97781	0.35	-0.85939	-0.37277
MA of Ped. L.	0.165192	-0.2801	0.94565	0.18434	0.98094	-0.06153	0.41043	0.85439	-0.31868
MA of Sup. Facet R.	-0.529928	-0.6982	0.48128	-0.63135	-0.6836	0.3662	-0.85258	-0.45569	-0.25582
MA of Sup. Facet L.	-0.336754	0.79087	0.511	0.61893	0.01023	0.78538	-0.66688	0.74373	-0.04634
MA of Inf. Facet R.	0.91116	0.39277	0.12458	0.75998	0.63875	0.12012	0.925	0.36061	-0.11974
MA of Inf. Facet L.	0.823772	-0.1404	0.54925	0.85869	-0.4262	0.28456	0.95697	-0.29019	0.00202
N. to Sup. Facet R.	-0.467238	0.71401	0.52142	-0.38263	0.68531	0.61963	-0.45482	0.40596	0.79267
N. to Sup. Facet L.	-0.57803	-0.602	0.55085	-0.51364	-0.7512	0.41456	-0.55544	-0.45466	0.69626
N. to Inf. Facet R.	0.406732	-0.8089	-0.42462	0.55388	-0.5398	-0.63391	0.207	-0.7425	-0.63706
N. to Inf. Facet L.	0.442936	0.76414	-0.46894	0.5125	0.71625	-0.47365	0.23877	0.78339	-0.57384
A. Dir. Of Ped. R.	-0.907985	-0.3996	0.12603	-0.97357	-0.2277	0.01723	-0.89528	-0.42397	0.13683
A. Dir. Of Ped. L.	-0.780696	0.54878	0.29892	-0.9821	0.18137	-0.05082	-0.77604	0.51078	0.36995
	AMNH# 98-174, 56yo, Bk. Male			AMNH# 98-217, 71yo, Wt. Male			AMNH# 98-246, 47yo, Bk. Male		
Description of Vector	x	y	z	x	y	z	x	y	z
MA of Ped. R.	0.383857	-0.8284	-0.40792	0.29838	0.05687	0.95275	NA	NA	NA
MA of Ped. L.	0.466618	0.82837	-0.30996	0.52961	0.81866	-0.22204	NA	NA	NA
MA of Sup. Facet R.	-0.516952	-0.7387	0.43258	-0.2245	-0.9577	0.18016	-0.55718	-0.72727	0.40079
MA of Sup. Facet L.	-0.543826	0.69103	0.47617	-0.31002	0.92426	0.22279	-0.90047	0.30067	-0.31425
MA of Inf. Facet R.	0.891714	0.30689	0.33266	-0.68401	-0.7292	-0.02061	0.82642	0.23214	0.51297
MA of Inf. Facet L.	0.849028	-0.5207	0.08964	-0.32292	0.87031	0.37185	0.8704	-0.24779	0.42545
N. to Sup. Facet R.	-0.578245	0.67395	0.45981	-0.74864	0.28785	0.59723	-0.52629	0.68261	0.50701
N. to Sup. Facet L.	-0.576365	-0.72	0.38658	-0.78236	-0.3812	0.49258	-0.37877	-0.89725	0.22689
N. to Inf. Facet R.	0.452189	-0.6353	-0.62599	0.6311	-0.5774	-0.51806	0.49522	-0.7332	-0.46603
N. to Inf. Facet L.	0.487857	0.70746	-0.51137	0.59644	0.4922	-0.63403	0.38579	0.88012	-0.27667
A. Dir. Of Ped. R.	-0.812599	-0.5129	0.27686	-0.85026	-0.4377	0.29241	NA	NA	NA
A. Dir. Of Ped. L.	-0.663831	0.55959	0.49617	-0.72722	0.57297	0.37796	NA	NA	NA
	AMNH# 98-295, 42yo, Wt. Male			AMNH# 98-320, 45yo, Wt. Male			AMNH# 98-324, 49yo, Wt. Male		
Description of Vector	x	y	z	x	y	z	x	y	z
MA of Ped. R.	0.43254	-0.8085	-0.39912	0.44223	-0.8059	-0.39373	0.39673	-0.86678	-0.30218
MA of Ped. L.	0.496524	0.78714	-0.36588	0.43473	0.83522	-0.33678	0.54002	0.77625	-0.32528
MA of Sup. Facet R.	-0.467581	-0.8167	0.3381	-0.332	-0.8498	0.40951			
MA of Sup. Facet L.	-0.805779	0.51244	-0.29685	-0.05671	0.82818	0.55759	-0.36091	0.679	0.6393
MA of Inf. Facet R.	0.809175	0.51062	0.2907	-0.70969	-0.7037	0.03348	0.90868	0.41132	0.07151
MA of Inf. Facet L.	0.687704	-0.7234	0.06188	0.78275	-0.4032	0.47403	0.87976	-0.47426	0.03319
N. to Sup. Facet R.	-0.622415	0.57579	0.53015	-0.69561	0.51378	0.50216			
N. to Sup. Facet L.	-0.591365	-0.7231	0.35696	-0.72195	-0.4198	0.55007	-0.62607	-0.68448	0.37354
N. to Inf. Facet R.	0.573977	-0.5811	-0.57691	0.62129	-0.6476	-0.44121	0.3795	-0.74241	-0.55209

Homo. Continued

Raw Vector Data									
	AMNH# 98-295, 42yo, Wt. Male			AMNH# 98-320, 45yo, Wt. Male			AMNH# 98-324, 49yo, Wt. Male		
Description of Vector	x	y	z	x	y	z	x	y	z
N. to Inf. Facet L.	0.640971	0.56494	-0.51962	0.60571	0.66852	-0.4315	0.45298	0.81498	-0.36141
A. Dir. of Ped. R.	-0.727338	-0.5745	0.37544	-0.77275	-0.5652	0.28884	-0.83245	-0.47845	0.27948
A. Dir. of Ped. L.	-0.654664	0.61637	0.43761	-0.70478	0.54834	0.45012	-0.62585	0.62877	0.46148
	AMNH# 98-327, 63yo, Wt. Male			AMNH# 98-333, 58yo, Wt. Male			AMNH# 98-99, 47yo, Wt. Female		
Description of Vector	x	y	z	x	y	z	x	y	z
MA of Ped. R.	0.277084	0.16413	0.94672	0.19631	0.36932	0.90833	NA	NA	NA
MA of Ped. L.	0.377997	0.83091	-0.4083	0.38899	0.86122	-0.32709	NA	NA	NA
MA of Sup. Facet R.	0.331514	-0.3078	0.89183	NA	NA	NA	0.18258	-0.4973	0.84815
MA of Sup. Facet L.	0.210123	0.47817	0.85276	-0.46559	0.82031	0.33214	-0.08619	0.76112	0.64286
MA of Inf. Facet R.	0.917028	0.35515	0.18146	0.58915	-0.0683	0.80514	0.87051	0.27316	0.40939
MA of Inf. Facet L.	0.848145	-0.5017	0.1701	0.81179	-0.2149	0.54298	0.75483	-0.36555	0.54462
N. to Sup. Facet R.	-0.535314	0.71702	0.44645	NA	NA	NA	-0.08149	0.85203	0.51712
N. to Sup. Facet L.	-0.770911	-0.4554	0.44532	-0.69258	-0.5714	0.44031	-0.71052	-0.49928	0.49586
N. to Inf. Facet R.	0.395497	-0.7512	-0.52852	0.47233	-0.7794	-0.4117	0.42671	-0.83339	-0.35126
N. to Inf. Facet L.	0.517115	0.71431	-0.47154	0.51166	0.70985	-0.48406	0.64054	0.58956	-0.49207
A. Dir. of Ped. R.	-0.80536	-0.4977	0.322	-0.77382	-0.5106	0.37484	NA	NA	NA
A. Dir. of Ped. L.	-0.76068	0.53013	0.37461	-0.8076	0.48962	0.32872	NA	NA	NA
	AMNH# 98-315, 65yo Bk. Female								
Description of Vector	x	y	z						
MA of Ped. R.	0.448193	-0.7965	-0.40585						
MA of Ped. L.	0.472769	0.80337	-0.36206						
MA of Sup. Facet R.	NA	NA	NA						
MA of Sup. Facet L.	-0.402228	0.73841	0.54127						
MA of Inf. Facet R.	0.757824	0.28566	0.5866						
MA of Inf. Facet L.	-0.35049	0.79254	0.49903						
N. to Sup. Facet R.	NA	NA	NA						
N. to Sup. Facet L.	-0.621201	-0.6544	0.43112						
N. to Inf. Facet R.	0.644962	-0.4639	-0.60732						
N. to Inf. Facet L.	0.552185	0.60524	-0.57339						
A. Dir. of Ped. R.	-0.639858	-0.6029	0.47657						
A. Dir. of Ped. L.	-0.649357	0.59537	0.47314						

Gorilla.

Raw Vector Data									
	AMNH# 90289, Male			AMNH# 167336, Male			AMNH# 167335, Male		
Description of Vector	x	y	z	x	y	z	x	y	z
MA of Ped. R.	0.123004	0.08752	0.98854	0.10109	0.12651	0.9868	0.29847	0.11771	0.94713
MA of Ped. L.	0.206535	-0.2949	0.93296	0.14711	-0.2724	0.95087	0.25925	-0.4447	0.85734
MA of Sup. Facet R.	-0.555758	-0.7772	0.29523	-0.46005	-0.8231	0.33309	-0.14254	-0.80451	0.57657
MA of Sup. Facet L.	-0.646692	0.55173	0.52668	-0.33819	0.79438	0.50457	-0.13565	0.41819	0.89818
MA of Inf. Facet R.	-0.822841	-0.5682	-0.01124	0.4056	0.02639	0.91367	0.44876	-0.15836	0.87951
MA of Inf. Facet L.	0.473646	-0.2999	0.82807	0.14267	0.0073	0.98974	NA	NA	NA
N. to Sup. Facet R.	-0.664696	0.62868	0.40366	-0.74093	0.56258	0.36677	-0.69033	0.49826	0.52457
N. to Sup. Facet L.	-0.531501	-0.8212	0.20765	-0.73432	-0.5581	0.38644	-0.58373	-0.76624	0.2686

Gorilla. Continued.

Raw Vector Data									
	AMNH# 90289, Male			AMNH# 167336, Male			AMNH# 167335, Male		
Description of Vector	x	y	z	x	y	z	x	y	z
N. to Inf. Facet R.	0.551469	-0.7936	-0.25712	0.45616	-0.8721	-0.17732	0.43927	-0.81798	-0.37141
N. to Inf. Facet L.	0.674831	0.72775	-0.12239	0.52585	0.84661	-0.08205	NA	NA	NA
A. Dir. of Ped. R.	-0.950125	-0.2773	0.14277	-0.90886	-0.3917	0.14333	-0.89962	-0.29671	0.32038
A. Dir. of Ped. L.	-0.866873	0.38703	0.31423	-0.9409	0.25795	0.21946	-0.82083	0.36634	0.43822
	AMNH# 90290, Male			AMNH# 201460, Male			AMNH# 81651, Male		
Description of Vector	x	y	z	x	y	z	x	y	z
MA of Ped. R.	0.206148	0.24282	0.94791	0.40205	0.05745	0.91381	0.57253	0.15358	0.80538
MA of Ped. L.	0.22276	-0.3029	0.92663	0.39388	-0.3348	0.85604	NA	NA	NA
MA of Sup. Facet R.	-0.670153	-0.5171	0.5325	0.30906	-0.4469	0.83948	0.48306	-0.59782	0.63973
MA of Sup. Facet L.	-0.563011	0.57459	0.59402	-0.51366	0.74089	0.43272	0.59325	0.67882	0.43274
MA of Inf. Facet R.	0.343504	-0.0753	0.93613	-0.56101	-0.6477	0.51555	0.4168	-0.43828	0.79636
MA of Inf. Facet L.	-0.78381	0.45357	0.42417	-0.14997	0.47247	0.8685	0.24969	0.25685	0.93364
N. to Sup. Facet R.	-0.391525	0.85576	0.33819	-0.47883	0.68953	0.54339	-0.30567	0.56952	0.76303
N. to Sup. Facet L.	-0.510736	-0.807	0.29652	-0.49136	-0.6675	0.55952	-0.5715	-0.02345	0.82026
N. to Inf. Facet R.	0.177614	-0.9736	-0.14343	0.51316	-0.7608	-0.39734	0.52647	-0.5978	-0.60454
N. to Inf. Facet L.	0.44211	0.88723	-0.13177	0.44599	0.81631	-0.36706	0.57709	0.73478	-0.35648
A. Dir. of Ped. R.	-0.932207	-0.2458	0.26569	-0.81059	-0.4418	0.38441	-0.76339	-0.25848	0.59197
A. Dir. of Ped. L.	-0.732501	0.57522	0.3641	-0.78974	0.35326	0.50152	NA	NA	NA
	AMNH# 214103, Male			AMNH# 54089, Male			AMNH# 54090, Male		
Description of Vector	x	y	y	x	y	z	x	y	z
MA of Ped. R.	0.332068	0.1249	0.93495	0.30302	0.14124	0.94246	0.40936	0.02153	0.91212
MA of Ped. L.	0.247312	-0.1598	0.95566	NA	NA	NA	0.49471	-0.14547	0.8568
MA of Sup. Facet R.	-0.40226	-0.6227	0.67119	0.00195	-0.595	0.8037	-0.71041	-0.63294	0.30775
MA of Sup. Facet L.	0.018459	0.72651	0.68691	NA	NA	NA	0.8147	-0.34713	0.46449
MA of Inf. Facet R.	-0.820166	-0.2488	0.51518	0.36189	-0.1297	0.92316	0.50503	0.24162	0.82859
MA of Inf. Facet L.	-0.665585	0.5112	0.54376	NA	NA	NA	0.59929	-0.46842	0.64918
N. to Sup. Facet R.	-0.44516	0.77364	0.4509	-0.53632	0.67771	0.50306	-0.49568	0.76039	0.41965
N. to Sup. Facet L.	-0.689308	-0.4884	0.53508	NA	NA	NA	-0.53841	-0.75029	0.38364
N. to Inf. Facet R.	0.177021	-0.9667	-0.18506	0.40616	-0.8694	-0.28132	0.85814	-0.2433	-0.4521
N. to Inf. Facet L.	0.473052	0.8525	-0.22241	NA	NA	NA	0.80051	0.34567	-0.48958
A. Dir. of Ped. R.	-0.937192	-0.0685	0.34202	-0.95085	0.11102	0.28908	-0.90374	0.1468	0.40213
A. Dir. of Ped. L.	-0.930957	0.23424	0.2801	NA	NA	NA	-0.8658	0.00285	0.50039
	AMNH# 99.1/1577, Male			AMNH# 54327, Female			AMNH# 167340, Female		
Description of Vector	x	y	z	x	y	z	x	y	z
MA of Ped. R.	0.184267	0.30092	0.93568	0.25612	0.30784	0.91632	0.13296	0.07039	0.98862
MA of Ped. L.	0.187111	-0.37	0.90998	0.06217	-0.2735	0.95985	0.19553	-0.25347	0.94738
MA of Sup. Facet R.	-0.61885	-0.6417	0.45301	0.07148	-0.4098	0.90939	-0.54127	-0.74053	0.39829
MA of Sup. Facet L.	-0.307662	0.64625	0.69836	-0.22834	0.70307	0.67347	-0.63225	0.53689	0.55858
MA of Inf. Facet R.	0.624217	-0.1385	0.76888	0.67167	0.03049	0.74022	-0.81519	-0.55679	0.15951
MA of Inf. Facet L.	NA	NA	NA	0.46998	0.09141	0.87793	0.53933	-0.14749	0.82908
N. to Sup. Facet R.	-0.485773	0.76586	0.42129	-0.50795	0.76969	0.38674	-0.66442	0.66698	0.33717
N. to Sup. Facet L.	-0.436482	-0.748	0.49993	-0.5637	-0.6595	0.49733	-0.50014	-0.83345	0.23499
N. to Inf. Facet R.	0.435759	-0.7551	-0.48979	0.45684	-0.8036	-0.38143	0.51867	-0.82435	-0.22679
N. to Inf. Facet L.	NA	NA	NA	0.46851	0.81712	-0.33589	0.37836	0.92201	-0.0821

Gorilla. Continued

Raw Vector Data									
	AMNH# 99.1/1577, Male			AMNH# 54327, Female			AMNH# 167340, Female		
Description of Vector	x	y	z	x	y	z	x	y	z
A. Dir. of Ped. R.	-0.959499	-0.1513	0.23762	-0.76732	-0.5118	0.3864	-0.90645	-0.39476	0.15002
A. Dir. of Ped. L.	-0.850838	0.40194	0.3384	-0.74409	0.62825	0.22724	-0.85697	0.42554	0.29072
	AMNH# 167339, Female			AMNH# 167337, Female			AMNH# 81652, Female		
Description of Vector	x	y	z	x	y	z	x	y	z
MA of Ped. R.	0.034384	0.18516	0.98211	0.18626	0.17048	0.9676	0.31645	0.17666	0.93202
MA of Ped. L.	-0.003492	-0.2988	0.95432	0.33053	-0.257	0.90814	0.3329	-0.23795	0.91245
MA of Sup. Facet R.	-0225022	-0.4334	0.87265	0.52927	0.0509	0.84693	-0.47442	-0.73073	0.49088
MA of Sup. Facet L.	0.008223	0.27295	0.96199	0.40538	0.1992	0.89218	-0.46925	0.63876	0.60975
MA of Inf. Facet R.	0.298767	-0.2569	0.91911	-0.69438	-0.4488	0.56255	0.3445	-0.1082	0.93253
MA of Inf. Facet L.	0.410187	0.02381	0.91169	-0.15653	0.14635	0.97677	-0.93425	0.30394	0.18653
N. to Sup. Facet R.	-.422773	0.85035	0.31333	-0.72611	0.54354	0.4211	-0.57304	0.67966	0.45792
N. to Sup. Facet L.	-.568668	-0.7926	0.22003	-0.78832	-0.418	0.4515	-0.45294	-0.76684	0.45475
N. to Inf. Facet R.	0.274102	-0.8994	-0.34046	0.45621	-0.8791	-0.13814	0.30934	-0.92478	-0.22157
N. to Inf. Facet L.	0.493566	0.83482	-0.24387	0.5116	0.85796	-0.04656	0.25688	0.93638	-0.23916
A. Dir. of Ped. R.	-.822847	-0.5525	0.13297	-0.97024	-0.1232	0.20847	-0.86766	-0.34325	0.35966
A. Dir. of Ped. L.	-.745638	0.63669	0.19659	-0.68358	0.59826	0.4181	-0.85958	0.32126	0.39739
	AMNH# 54091, Female			AMNH# 99.1/1578, Female					
Description of Vector	x	y	z	x	y	z			
MA of Ped. R.	0.046485	0.19536	0.97963	0.37877	0.3591	0.85299			
MA of Ped. L.	0.132641	-0.2112	0.9684	0.35765	-0.1945	0.91337			
MA of Sup. Facet R.	-0.697589	-0.6704	0.25295	-0.71269	-0.4339	0.5512			
MA of Sup. Facet L.	0.338823	0.11258	0.93409	-0.74712	0.5054	0.43174			
MA of Inf. Facet R.	-0.235297	-0.8761	0.42092	0.3751	-0.0257	0.92663			
MA of Inf. Facet L.	0.355317	-0.0754	0.9317	0.4526	-0.0829	0.88785			
N. to Sup. Facet R.	-0.617502	0.74155	0.26228	-0.32785	0.90069	0.28509			
N. to Sup. Facet L.	-0.523832	-0.8021	0.28669	-0.40422	-0.8611	0.30848			
N. to Inf. Facet R.	0.872306	-0.3813	-0.30604	0.61135	-0.7445	-0.26814			
N. to Inf. Facet L.	0.802694	0.53536	-0.26282	0.74361	0.58461	-0.32447			
A. Dir. of Ped. R.	-0.997251	-0.0476	0.05681	-0.92408	0.09577	0.37002			
A. Dir. of Ped. L.	-0.946888	0.26175	0.18679	-0.92985	0.01635	0.36758			

Pan.

Raw Vector Data, *Pan* Sample									
	AMNH# 51377, Male			AMNH# 51278, Male			AMNH# 174861, Male		
Description of Vector	x	y	z	x	y	z	x	y	z
MA of Ped. R.	0.437118	0.279958	0.854723	0.385527	0.167147	0.907431	0.341573	0.157836	0.926507
MA of Ped. L.	0.380015	-0.24063	0.893133	0.317779	-0.24027	0.917217	0.317087	-0.35364	0.879997
MA of Sup. Facet R.	0.236742	-0.20905	0.948816	0.036721	-0.36084	0.931903	0.058365	-0.28476	0.956821
MA of Sup. Facet L.	0.183441	0.225498	0.956818	0.023484	0.279007	0.960002	-0.16172	0.395314	0.904198
MA of Inf. Facet R.	0.629024	-0.01281	0.777281	0.759219	0.015771	0.650644	0.515149	0.000552	0.8571
MA of Inf. Facet L.	0.506402	0.01236	0.862209	0.690194	-0.10721	0.715638	0.558144	-0.07621	0.826237
N. to Sup. Facet R.	-0.45975	0.836215	0.298956	-0.34446	0.870813	0.350763	-0.37202	0.883214	0.285544
N. to Sup. Facet L.	-0.504355	-0.81387	0.288505	-0.30254	-0.91326	0.272822	-0.45914	-0.84119	0.285647
N. to Inf. Facet R.	0.20357	-0.96226	-0.18061	0.311	-0.88698	-0.3414	0.301933	-0.93601	-0.18087

Pan. Continued

Raw Vector Data									
	AMNH# 51377, Male			AMNH# 51278, Male			AMNH# 174861, Male		
Description of Vector	x	y	z	x	y	z	x	y	z
N. to Inf. Facet L.	0.320591	0.925524	-0.20156	0.358357	0.909816	-0.20932	0.333991	0.932175	-0.13964
A. Dir. of Ped. R.	-0.846491	-0.19309	0.496154	-0.92158	0.021486	0.387583	-0.83146	-0.40885	0.376183
A. Dir. of Ped. L.	-0.852023	0.284802	0.439255	-0.85708	0.340913	0.386249	-0.76193	0.457529	0.458408
	AMNH# 51379, Male			AMNH# 51202, Male			AMNH# 51392, Male		
Description of Vector	x	y	z	x	y	z	x	y	z
MA of Ped. R.	0.307012	0.266302	0.913689	0.317965	0.15459	0.935414	0.264879	0.221105	0.93859
MA of Ped. L.	0.325353	-0.24053	0.914489	0.321483	-0.25284	0.912536	0.340492	-0.37802	0.860908
MA of Sup. Facet R.	0.216414	-0.32202	0.921665	0.100986	-0.28317	0.953739	0.022741	-0.28273	0.958929
MA of Sup. Facet L.	0.078224	0.305897	0.948846	0.466869	0.192864	0.863039	-0.88553	0.31371	-0.34266
MA of Inf. Facet R.	0.367143	-0.1811	0.912365	0.541253	-0.02866	0.840371	0.695159	-0.02214	0.718515
MA of Inf. Facet L.	0.519744	0.107518	0.84753	0.568858	0.004627	0.822423	0.704297	-0.02241	0.709552
N. to Sup. Facet R.	-0.101073	0.931574	0.349218	-0.40142	0.865544	0.299485	-0.21273	0.935843	0.28097
N. to Sup. Facet L.	-0.254778	-0.91402	0.315675	-0.44836	-0.78957	0.418989	-0.44352	-0.7904	0.422562
N. to Inf. Facet R.	0.288291	-0.91041	-0.29672	0.259326	-0.94501	-0.19925	0.250903	-0.92919	-0.27138
N. to Inf. Facet L.	0.349932	0.878219	-0.32601	0.318589	0.920669	-0.22554	0.325162	0.898674	-0.29437
A. Dir. of Ped. R.	-0.814204	-0.42359	0.397042	-0.87976	-0.3197	0.351881	-0.85035	-0.40542	0.335481
A. Dir. of Ped. L.	-0.840999	0.36851	0.396133	-0.82156	0.404699	0.401563	-0.70215	0.506734	0.500208
	AMNH# 81854, Unk.			AMNH# 51381, Unk.			AMNH# 51394, Unk.		
Description of Vector	x	y	z	x	y	z	x	y	z
MA of Ped. R.	0.550067	0.233764	0.801736	0.422411	0.23281	0.875996	0.47507	0.066673	0.877419
MA of Ped. L.	0.535515	-0.14146	0.832594	0.460736	-0.37385	0.80496	0.365075	-0.35178	0.86196
MA of Sup. Facet R.	0.070312	-0.33421	0.939874	0.092389	-0.51697	0.851003	0.280848	-0.49518	0.822141
MA of Sup. Facet L.	0.416969	0.270371	0.867777	-0.55517	0.712299	0.429434	-0.56567	0.638867	0.521408
MA of Inf. Facet R.	0.414836	-0.06111	0.907842	0.604408	-0.05841	0.794531	0.535665	-0.18963	0.822862
MA of Inf. Facet L.	0.448901	0.21927	0.866261	0.570545	-0.00607	0.821244	0.610939	-0.0586	0.789506
N. to Sup. Facet R.	-0.318183	0.885475	0.338666	-0.33179	0.789832	0.515831	-0.49847	0.656761	0.565855
N. to Sup. Facet L.	-0.596845	-0.63861	0.485754	-0.54625	-0.70161	0.457558	-0.5266	-0.76644	0.367786
N. to Inf. Facet R.	0.389974	-0.88952	-0.23807	0.355493	-0.87274	-0.33459	0.337957	-0.84487	-0.41471
N. to Inf. Facet L.	0.520409	0.723908	-0.45292	0.430957	0.853448	-0.29309	0.49759	0.804077	-0.32537
A. Dir. of Ped. R.	-0.784343	-0.18504	0.592086	-0.84717	-0.24225	0.472891	-0.78825	-0.41096	0.458017
A. Dir. of Ped. L.	-0.724142	0.430376	0.538883	-0.75992	0.302397	0.575397	-0.75176	0.434751	0.495828
	AMNH# 90189, Unk.			AMNH# 90191, Unk.			AMNH# 167341, Unk.		
Description of Vector	x	y	z	x	y	z	x	y	z
MA of Ped. R.	0.330696	0.179255	0.926557	0.264501	0.265718	0.927056	0.375816	0.106039	0.920607
MA of Ped. L.	0.284985	-0.35495	0.89039	0.171031	-0.43069	0.886145	0.384584	-0.27468	0.881277
MA of Sup. Facet R.	0.492565	-0.17921	0.851625	-0.15154	-0.33697	0.929239	-0.53407	-0.5213	0.665589
MA of Sup. Facet L.	0.374429	0.033189	0.926661	-0.02959	0.331368	0.943038	-0.45348	0.513835	0.728239
MA of Inf. Facet R.	0.697442	-0.06356	0.713817	0.339338	-0.04085	0.939777	0.399262	-0.1596	0.902838
MA of Inf. Facet L.	-0.677869	0.49778	0.541026	0.275515	-0.00883	0.961256	0.540192	-0.01432	0.84142
N. to Sup. Facet R.	-0.193346	0.931579	0.30786	-0.38121	0.887295	0.259595	-0.40845	0.848396	0.336737
N. to Sup. Facet L.	-0.33851	-0.92549	0.169926	-0.60944	-0.75379	0.245748	-0.40688	-0.84632	0.343784
N. to Inf. Facet R.	0.180364	-0.94843	-0.26067	0.37246	-0.91157	-0.17411	0.36183	-0.87737	-0.31511
N. to Inf. Facet L.	0.490501	0.854392	-0.17153	0.555666	0.817439	-0.15175	0.202823	0.972597	-0.11366
A. Dir. of Ped. R.	-0.890747	-0.26507	0.369197	-0.93132	-0.17919	0.317078	-0.851	-0.35375	0.388147

Pan. Continued

Raw Vector Data									
	AMNH# 90189, Unk.			AMNH# 90191, Unk.			AMNH# 167341, Unk.		
Description of Vector	x	y	z	x	y	z	x	y	z
A. Dir. of Ped. L.	-0.829607	0.373966	0.41461	-0.80685	0.454951	0.376846	-0.89148	0.137182	0.431793
	AMNH# 167342, Unk.			AMNH # 167343, Unk.			AMNH# 167346, Unk.		
Description of Vector	x	y	z	x	y	z	x	y	z
MA of Ped. R.	0.362846	0.109064	0.925445	0.524503	0.185839	0.83088	0.168865	0.247432	0.954076
MA of Ped. L.	0.450944	-0.15561	0.878883	0.473631	-0.42566	0.771031	0.274117	-0.24688	0.929468
MA of Sup. Facet R.	0.586252	-0.12097	0.801046	0.090002	-0.35277	0.931371	0.003336	-0.09244	0.995712
MA of Sup. Facet L.	0.511312	0.012676	0.859302	0.141493	0.392407	0.908843	-0.54215	0.423273	0.725889
MA of Inf. Facet R.	0.814039	0.079754	0.575309	0.926036	0.129184	0.354638	0.103358	0.033597	0.994077
MA of Inf. Facet L.	-0.305927	0.43667	0.846007	0.859116	-0.21065	0.466419	0.777663	-0.19955	0.596171
N. to Sup. Facet R.	-0.30701	0.881863	0.357859	-0.21465	0.906319	0.364024	-0.39259	0.915654	0.086326
N. to Sup. Facet L.	-0.550089	-0.76339	0.338582	-0.38765	-0.8228	0.415607	-0.4335	-0.88092	0.189896
N. to Inf. Facet R.	0.267955	-0.93038	-0.25017	0.282479	-0.86038	-0.4242	0.384448	-0.9231	-0.00877
N. to Inf. Facet L.	0.378159	0.871241	-0.31295	0.388925	0.861102	-0.32747	0.405398	0.883967	-0.23293
A. Dir. of Ped. R.	-0.857752	-0.349	0.377436	-0.73734	-0.38881	0.552416	-0.89123	-0.37507	0.255013
A. Dir. of Ped. L.	-0.790336	0.387948	0.4742	-0.67694	0.38409	0.627875	-0.86229	0.364838	0.351211
	AMNH# 54330, Unk.			AMNH# 174860, Unk			AMNH# Unk., Unk.		
Description of Vector	x	y	z	x	y	z	x	y	z
MA of Ped. R.	0.473025	0.056875	0.879211	0.321498	0.106226	0.940933	0.48209	0.225415	0.846627
MA of Ped. L.	0.431014	-0.03341	0.901726	0.333581	-0.28208	0.899529	0.46998	-0.29634	0.831444
MA of Sup. Facet R.	-0.039516	-0.27455	0.960761	0.238388	-0.16465	0.957112	-0.43005	-0.46848	0.771738
MA of Sup. Facet L.	-0.121767	0.44288	0.888274	-0.39422	0.315211	0.863268	-0.5284	0.660935	0.532879
MA of Inf. Facet R.	-0.640971	-0.56817	0.516085	0.597732	0.115512	0.79333	0.634349	-0.08663	0.768177
MA of Inf. Facet L.	0.743024	-0.17555	0.645832	0.519948	-0.03566	0.853453	0.675502	-0.09531	0.731172
N. to Sup. Facet R.	-0.400064	0.885429	0.236566	-0.45193	0.853509	0.259386	-0.29999	0.880404	0.367283
N. to Sup. Facet L.	-0.370872	-0.85041	0.373163	-0.27316	-0.93708	0.21742	-0.45555	-0.75037	0.47897
N. to Inf. Facet R.	0.536677	-0.81244	-0.22788	0.219861	-0.97524	-0.02365	0.281122	-0.89981	-0.33363
N. to Inf. Facet L.	0.457564	0.837474	-0.29879	0.158522	0.985801	-0.05538	0.412996	0.870379	-0.26809
A. Dir. of Ped. R.	-0.871405	-0.11705	0.476397	-0.84069	-0.42526	0.335256	-0.83663	-0.16842	0.521238
A. Dir. of Ped. L.	-0.828614	0.380983	0.410184	-0.83378	0.357002	0.42115	-0.66368	0.502373	0.554209

Pongo.

Raw Vector Data									
	AMNH# 61586, Male			AMNH# 238487, Male			AMNH# 140246, Male		
Description of Vector	x	y	z	x	y	z	x	y	z
MA of Ped. R.	0.08109	0.166519	0.982698	NA	NA	NA	0.111743	0.319078	0.941118
MA of Ped. L.	NA	NA	NA	NA	NA	NA	NA	NA	NA
MA of Sup. Facet R.	0.256731	-0.79678	0.547027	0.284882	-0.71853	0.634471	0.322088	-0.08601	0.942794
MA of Sup. Facet L.	0.400035	0.129814	0.90726	0.413573	0.222408	0.882889	0.147248	0.136135	0.979686
MA of Inf. Facet R.	0.565543	-0.2728	0.778292	0.538296	-0.18348	0.822541	0.297263	-0.22971	0.926752
MA of Inf. Facet L.	0.465343	-0.01891	0.884928	0.447483	0.179745	0.876043	0.541475	0.208685	0.814405
N. to Sup. Facet R.	-0.757461	0.185666	0.625924	-0.76236	0.231406	0.60437	-0.63264	0.721301	0.281935
N. to Sup. Facet L.	-0.665756	-0.63917	0.385004	-0.6676	-0.58529	0.460163	-0.40088	-0.89727	0.184936
N. to Inf. Facet R.	0.745713	-0.23391	-0.62386	0.763734	-0.30643	-0.56816	0.461009	-0.81546	-0.34999
N. to Inf. Facet L.	0.67332	0.656516	-0.34004	0.644576	0.614207	-0.45527	0.236317	0.891866	-0.38565

Pongo. Continued

Raw Vector Data									
	AMNH# 61586, Male			AMNH# 238487, Male			AMNH# 140246, Male		
Description of Vector	x	y	z	x	y	z	x	y	z
A. Dir. of Ped. R.	-0.909372	-0.39124	0.141335	NA	NA	NA	-0.78734	-0.54939	0.279751
A. Dir. of Ped. L.	NA	NA	NA	NA	NA	NA	NA	NA	NA
	AMNH# 28252, Male			AMNH# 28253, Unk.					
Description of Vector	x	y	z	x	y	z			
MA of Ped. R.	0.40951	0.150059	-0.96389	-0.21999	0.058964	0.910398			
MA of Ped. L.	0.261747	0.432109	0.831914	-0.34814	-0.15328	0.952888			
MA of Sup. Facet R.	0.388142	-0.093279	-0.67987	0.727377	-0.506	0.770269			
MA of Sup. Facet L.	0.284891	0.431487	0.361134	0.826681	0.640942	0.712763			
MA of Inf. Facet R.	0.479223	0.51462	-0.30385	0.801773	-0.2302	0.846966			
MA of Inf. Facet L.	0.637168	0.683651	0.095752	0.7235	0.298844	0.710429			
N. to Sup. Facet R.	-0.65829	-0.65802	0.590363	0.46742	0.432709	0.615967			
N. to Sup. Facet L.	-0.61944	-0.751262	-0.36347	0.550904	-0.44436	0.647176			
N. to Inf. Facet R.	0.440951	0.57948	-0.56596	-0.58643	-0.77122	-0.45911			
N. to Inf. Facet L.	0.446346	0.507396	0.650199	-0.5655	0.608383	-0.65624			
A. Dir. of Ped. R.	-0.88338	-0.91495	-0.2197	0.338523	-0.22368	0.411843			
A. Dir. of Ped. L.	-0.7947	-0.803535	0.530423	0.270154	0.526022	0.302908			

LIST OF REFERENCES

Adams MA and WC Hutton (1980) The effect of posture on the role of the apophysial joints in resisting intervertebral compressive forces. The Journal of Bone and Joint Surgery. 62-B: 358-362.

Begun DR (1992) Miocene fossil hominids and the chimp-human clade. Science. 257: 248-265.

Beiwener AA, Fazzalari NL, Konieczynski DD, Baudinette RV (1996) Adaptive changes in trabecular architecture in relation to functional strain patterns and disuse. Bone. 19: 1-8.

Bertram JEA and Swartz SM (1991) The "Law of Bone Transformation": A case of crying Wolff? Biology Review. 66: 245-273.B

Bongnuk N and Twomey L (1987) Clinical Anatomy of the Lumbar Spine. Churchill Livingstone, New York.

Brukner P, Bennell K, Matheson G (1999) Stress Fractures. Blackwell Science Asia, Champaign.

Burkus JK (1990) Unilateral spondylolysis associated with spina bifida occulta and nerve root compression. Spine. 15: 555-559

Carter DR, Harris WH, Vasu R, Caler WE (1981) The mechanical and biological response of cortical bone to in vivo strain histories. In Mechanical Properties of Bone. Cowin SC (ed.). American Society of Mechanical Engineers, New York.

Chamay A and Tschantz P (1972) Mechanical influences in bone remodeling. Experimental research on Wolff's law. Journal of Biomechanics. 5: 173.

Cullinane DM and Einhorn TA (2002) Biomechanics of bone. In Principles of Bone Biology. Second Edition. Bilezikian JP, Raisz LG, Rodan GA (eds.). Academic Press, New York City.

Davis PR (1961) Human lower lumbar vertebrae: some mechanical and osteological considerations. Journal of Anatomy. 95: 337-344.

Demes B, Jungers WL, and Walker C (2000) Cortical bone distribution in the femoral neck of strepsirrhine primates. Journal of Human Evolution. 39: 367-379.

Dixon AF (1981) The Natural History of the *Gorilla*. Columbia University Press, New York.

Doran D (1989) Chimpanzee and pygmy chimpanzee positional behavior: the influence of environment, body size, morphology and ontogeny on locomotion and posture. PhD Dissertation, The State University of New York at Stony Brook, Stony Brook, NY.

Duncan AS, Kappelman J, and Shaprio LJ (1994) Metatarsophalangeal joint function and positional behavior in *Australopithecus afarensis*. American Journal of Physical Anthropology. 93: 67-81.

El-Bohy AA, Yang KH, and King AI (1989) Experimental verification of facet load transmission by direct measurement of the facet lamina contact pressure. Journal of Biomechanics. 22: 931-941.

Fleagle JG (1988) Primate Adaptation and Evolution. Academic Press, San Diego.

Fyrie DP and Carter DR (1986) A unifying principle relating to stress to trabecular bone morphology. Journal of Orthopaedic Research. 4: 304-317.

Hallgrimsson B, Willmore K, and Hall BK (2002) Canalization, developmental stability, and morphological intergration in primate limbs. American Journal of Physical Anthropology. Supplement 35: 131-158.

Heinrich RE, Rose MD, Leakey RE, Walker AC (1993) Hominid radius from the middle Pliocene of Lake Turkana, Kenya. American Journal of Physical Anthropology. 2: 139-148.

Holdsworth FW (1963) Fractures, dislocations, and fracture-dislocations of the spine. Journal of Bone and Joint Surgery. 45B: 6-20.

Hunt KD (1991) Mechanical implications of chimpanzee positional behavior. American Journal of Physical Anthropology. 86: 521-536.

Kimura T (2003) Differentiation between fore and hindlimb bones and locomotor behavior in primates. Folia Primotologia. 74: 17-32.

Kip PC, Esses SI, Doherty BI, Alexander JW, Crawford MJ**.** (1994) Biomechanical testing of pars defect repairs. Spine. 19: 2692-2697.

Koop BF, Tagle DA, Goodman M, Slightom JL. (1989) A molecular view of primate phylogeny and important systematic and evolutionary questions. Molecular Biology and Evolution. 6: 580-612.

Latimer B and Lovejoy CO (1990a) Metatarsalphalangeal joints of *Australopithecus afarensis*. American Journal of Physical Anthropology. 83: 13-23.

Latimer B and Lovejoy CO (1990b) Hallucal tasrsometatarsal joint in *Australopithecus afarensis*. American Journal of Physical Anthropology. 82: 125-133.

Lockwood CA, Kimbel WH, and Lynch JM (2004) Morphometerics and hominoid phylogeny: Support for a chimpanzee-human clade and differentiation among greaet apes subspecies. Proceedings of the National Academy of Sciences of the United States of America. 101: 4356-4360.

Lovejoy CO (1975) Biomechanical perspectives on the lower limb of early hominids. In Primate Functional Morphology and Evolution. Tuttle RH (ed.). Mouton, Paris.

Lovejoy CO (1979) A reconstruction of the pelvis of AL-288 (Hadar Formation, Ethiopia). American Journal of Physical Anthropology. 50: 460.

Lovejoy CO (1988) The evolution of human walking. Scientific American. 259: 118-125.

Mardia KV and Jupp PE (2000) Directional Statistics. Wiley Press, New York.

Martin RB (2000) Toward a unifying theory of bone remodeling. Bone. 26: 1-6.

Mullender MG and Huiskes R (1995) Proposal for the regulatory mechanism of Wolff's Law. Journal of Orthopaedic Research. 13: 503-512.

Mundy GR (1999) Bone Remodeling and Its Disorders. Martin Dunitz, Ltd, London

Ohman JC, Krichta TJ, Lovejoy CO, Mensforth RP and Latimer B (1997) Cortical bone distribution in the femoral neck of hominids: Implications for the locomotion of *Australopithecus afarensis*. American Journal of Physical Anthropology. 104: 117-131.

Ozkaya N and Nordin M (1999) Fundamentals of Biomechanics: Equilibrium, Motion, and Deformation. Second Edition. Springer, New York.

Pal GP and Routal RV (1986) A study of weight transmission through the cervical and upper thoracic regions of the vertebral column in man. Journal of Anatomy. 148: 245-261.

Pal GP and Routal RV (1987) Transmission of weight through the lower thoracic and lumbar regions of the vertebral column in man. Journal of Anatomy. 152: 93-105

Pearson OM and Lieberman DE (2004) "The aging of Wolff's "Law": Ontogeny and responses to mechanical loading in cortical bone." Yearbook of Physical Anthropology. 47: 63-99.

Panjabi MM and White MA (2001) Biomechanics in the Musculoskeletal System. Churchill Livingstone, New York.

Prasad P, King AI, Ewing CL. (1974) The role of articular facets during +Gz acceleration. Journal of Applied Mechanics. P321-326.

Rumcheva P and Presnell B (2005) Projected Multivariate Linear Models for Directional Data: Multi-Sample Tests of Hypotheses, Technical Report Number: 2005-007. Department of Statistics, University of Florida.

Ruvolo M (1997) Molecular phylogeny of the hominoids: Inferences from multiple independent DNA sequence data sets. Molecular Biology and Evolution. 14: 248-265.

Salem A, Ray DA, Xing J, Callin PA, Myers JS, Hedges DJ, Garber RK, Witherspoon DJ, Jorde LB, Batzer MA. (2003) Alu elements and hominid phylogenetics. Proceedings of the National Academy of Sciences of the United States of America. 100: 12787-12791.

Sanders WJ (1995) Function, Allometry, and Evolution of the Australopithecine Lower Precaudal Spine. PhD Dissertation, New York University.

Sanders WJ (1998) Comparative morphometric study of the *Australopithecus* vertebral series Stw-H8/H41. Journal of Human Evolution. 34: 249-302.

Satta Y, Klein J, and Takahata N. (2000) DNA archives and our nearest relative: The trichotomy revisited. Molecular Phylogenetics and Evolution. 14: 259-275.

Scaffler MB (2000) Bone fatigue and remodeling in the development of stress fractures. In Musculoskeletal Fatigue and Stress Fractures. Burr DB and Milgrom C (eds.). CRC Press, New York.

Schmitt D (1994) Forelimb mechanics as a function of substrate type during quadrupedalism in two anthropoid primates. Journal of Human Evolution. 26: 441-457.

Schmitt D (2003) "Substrate size and primate forelimb mechanics: implications for understanding the evolution of primate locomotion. International Journal of Primatology. 24: 1023-1036.

Schultz A, Andersson G, Örtengren R, Haderspeck K, and Nachemson A. (1982) Loads on the lumbar spine: validation of a biomechanical analysis by measurements of intradiscal pressure and myoelectric signals. The Journal of Bone and Joint Surgery. 64A: 713-720.

Schultz AH (1961) The vertebral column and thorax. Primotologia. 5: 1-66.

Schultz AH (1941) Growth and development of the orang-utan. Contributions to Embryology. 182:58-111.

Semon RL and D Spengler. (1981) Significance of lumbar spondylolysis in college football players. Spine. 6:172-4.

Shapiro LJ (1991) Functional Morphology of the Primate Spine with Special Reference to Orthograde Posture and Bipedal Locomotion. PhD Dissertation, State University of New York at Stony Brook.

Shapiro LJ (1993) Evaluation of "unique" aspects of human vertebral bodies and pedicles with a consideration of Australopithecus africanus. Journal of Human Evolution. 25: 433-470.

Shapiro LJ (1995) Functional morphology of *Indrid* lumbar vertebrae. American Journal of Physical Anthropology 98: 323-342.

Shapiro LJ and Johnson SE (1998) Positional behavior and vertebral morphology in atelines and cebines. American Journal of Physical Anthropology. 105: 333-354.

Shapiro LJ, Demes B, Cooper J. (2001) Lateral bending of the lumbar spine during quadrupedalism in strepsirhines. Journal of Human Evolution. 40: 231-259.

Shapiro LJ and Simons CVM (2002) Functional aspects of strepsirrhine lumbar vertebral bodies and spinous processes. Journal of Human Evolution. 42: 753-783.

Shoshani J**,** Groves CP, Simons EL, Gunnell GF. (1996) Primate phylogeny: morphometric vs. molecular results. Molecular Phylogenetics and Evolution. 5: 102-154.

Sugardjito J (1982) Locomotor behavior of the Sumatran orangutan (*Pongo pygmaeus abelli*) at Ketambe, Gunung Leuser National Park. Malaysian Nature Journal 35: 57-64.

Sugardjito J and van Hooff J (1986) Sex-age differences in positional behavior of Sumatran orangutan (*Pongo pygmaeus abelli*) in the Gunung Leuser National Park, Indonesia. Folia Primatologica. 47: 14-25.

Susman RL, Stern JT, and Jungers WL (1984) Aboreality and bipedality in the Hadar hominids. Folia Primatologia. 43: 113-156.

Susman RL and Demes AB (1994) Relative foot length in *Australopithecus afarensis* and its implications for bipedality. American Journal of Physical Anthropology. Supplement. 18: 192.

Turner CH and Pavalko FM (1998) Mechanotransduction and functional response of the skeleton to physical stress: The mechanisms and mechanics of bone adaptation. Journal of Orthopaedic Science. 3: 346-355.

Tuttle RH (1985) Ape footprints and Laetoli impressions: A response to SUNY claims. In Hominid Evolution Past, Present and Future. Tobia PV (ed.). Alan R. Liss, New York.

Tuttle RH and Watts DP (1985) The positional behavior and adaptive complexes of *Pan gorilla.* In Primate Morphophysiology, Locomotor Analyses and Human Bipedalism. Kondo S (ed.). University of Tokyo Press, Tokyo.

Velte MJ (1987) A New Biomechanical Model of the Vertebral Column in Anthropoid Primates. PhD Dissertation, University of Chicago

Wainwright SA (1988) Form and function in organisms. American Zoology. 28: 671-680.

Yerby SA and DR Carter (2000) Bone fatigue and stress fractures. In Musculoskeletal Fatigue and Stress Fractures. Burr DB and Milgrom C (eds.). CRC Press, New York.

Yocum TR and Rowe LJ (2005) Essentials of Skeletal Radiology, Third Edition, Vol.1. Lippincott, Williams, and Wilkins, Philadelphia.

BIOGRAPHICAL SKETCH

Dorion Amanda Keifer was born in Idaho Falls, Idaho, on April 20th, 1979. She received her bachelor's degree in anthropology from New York University in 2000.